

SMALL STRUCTURES VIA THERMAL INSTABILITY OF PARTIALLY IONIZED PLASMA I. CONDENSATION MODE

TSUBASA FUKUE AND HIDEYUKI KAMAYA ¹

Department of Astronomy, School of Science, Kyoto University, Kyoto 606-8502, Japan

tsubasa@kusastro.kyoto-u.ac.jp

ABSTRACT

Thermal instability of partially ionized plasma is investigated by means of a linear perturbation analysis. According to the previous studies under the one fluid approach, the thermal instability is suppressed due to the magnetic pressure. However, the previous studies did not precisely consider the effect of the ion-neutral friction, since they did not treat the flow as two fluid which is composed of ions and neutrals. Then, we revisit the effect of the ion-neutral friction of the two fluid to the growth of the thermal instability. According to our study, the characteristic features of the instability are the following four points: (1) The instability which is characterized by the mean molecular weight of neutrals is suppressed via the ion-neutral friction only when the magnetic field and the friction are sufficiently strong. The suppression owing to the friction occurs even along the field line. If the magnetic field and the friction are not so strong, the instability is not stabilized. (2) The effect of the friction and the magnetic field is mainly reduction of the growth rate of the thermal instability of weakly ionized plasma. (3) The effect of friction does not affect the critical wavelength λ_F for the thermal instability. This yields that λ_F of the weakly ionized plasma is not enlarged even when the magnetic field exists. We insist that the thermal instability of the weakly ionized plasma in the magnetic field can grow up even at the small length scale where the instability under the assumption of the one fluid plasma can not grow owing to the stabilization by the magnetic field. (4) The wavelength of the maximum growth rate of the instability shifts shortward

¹Current address: Department of Earth and Ocean Sciences, School of Applied Sciences, National Defense Academy of Japan, Yokosuka 239-8686, Japan

according to the decrement of the growth rate. This is because the friction is effective at rather larger scale. Therefore, smaller structures are expected to appear than those without the ion-neutral friction. Our results indicate the friction with the magnetic field affects the morphology and evolution of the interstellar matter. In summary, the ion-neutral friction is important for the evaluation of the thermal instability in weakly ionized plasma along and perpendicular to the magnetic field.

Subject headings: instabilities — ISM: evolution

1. INTRODUCTION

The recent progress of the interstellar medium (ISM) observations has established that the small and tiny scale structures of ISM is very ubiquitous. Historically, the initial observational target is the neutral phase of ISM. Indeed, the tiny scale structures are discovered by 21 cm absorption line observations against quasars with VLBI techniques (Dieter et al. 1976). The results are confirmed by Diamond et al. (1989). To look for the small scale structures in the cold neutral phase of the ISM furthermore, the observations of 21 cm absorption lines have been also performed against pulsars (Frail et al. 1994). Meyer et al. (1996) observe optical spectral lines to find small structures against close binary stars. The images of the small-scale H I have been taken with the MERLIN array (Davis et al. 1996). These results are established by higher angular resolution observations with VLBA and VLA toward quasars (Faison et al. 1998; Faison & Goss 2001), which show small clumps on the order of a few AU in neutral Galactic H I clouds. Cold H I clouds have significant structure in subparsec scales (Gibson 2000; Brogan et al. 2005). Such small and tiny scale structures has been detected in the local interstellar medium as H I absorption lines, although their column density is very small (Braun & Kanekar 2005).

In addition to the small and tiny scale structures of H I cloud, the picture of the planetary nebula NGC 7293 shows fine small structures and knots (Rodríguez et al. 2002; O’Dell et al. 2004). Even in the starforming regions, there are variety small scale structures. For example, Langer et al. (1995) observe some clumps with size from 0.007 to 0.021 pc in the Taurus Molecular Cloud 1 (TMC1), in particular, core D. The mass of these fragments is estimated to be $\lesssim 0.01 - 0.15 M_{\odot}$. SPITZER has begun producing higher spatial resolution mid-infrared maps (Churchwell et al. 2004), and revealed the fine structure of the starforming region. We think that it is possible for proto-brown dwarfs of $< 0.08 M_{\odot}$ to exist there. A high resolution observation in future is expected to reveal hidden, small structures, as well as substellar objects with very small mass. In any ways, the tiny-scale structure seems to be

ubiquitous, not associated with large extinction (Heiles 1997).

To study the origin of the small-scale structures of ISM is important to understand the evolution of and structure formation in ISM. Especially, in the starforming regions, the small, low-mass structures can relate to the low-mass cutoff of the initial mass function, the coagulation unit to form the massive stars, and so on. Then, we should investigate the physical origin of these small and tiny structures in the partially ionized medium, since the cold H I and molecular clouds are weakly ionized. By the way, it is not easy for the small and tiny scale structure to form as a result of gravitational instability since their size is much smaller than the Jeans length. According to Langer et al. (1995), indeed, the small-scale structures appear to be gravitationally unbound. This suggests that some fragmentation mechanisms but pure Jeans gravitational instability may be important in the clouds. We expect the thermal instability as this mechanism, and revisit it in this paper.

The basics of the thermal instability has been summarized in Field (1965). When the following condition is satisfied, the system is thermally unstable: If the cooling becomes efficient as the temperature decreases, the thermal energy gets lost more and more. If the cooling becomes efficient during the fluid contraction, the system shrinks on and on. Importantly, the critical length scale of the thermal instability is smaller than that of the dynamical instability like the Jeans instability. That is, even if a system is stable against the gravitational instability, the system can become thermally unstable. Then, the thermal instability can be the physical origin of the smaller-scale formation than the dynamical instability. Indeed, Koyama & Inutsuka (2002) propose that the clumpiness in clouds emerges naturally from their formation through the thermal instability. Their two-dimensional calculations follow the fragmentation into small cloudlets that result from the thermal instability in a shock-compressed layer. Burkert & Lin (2000) investigate the cooling and fragmentation of optically thin gas with a power-law cooling function. According to them, small-scale perturbations have the potential to reach higher amplitude than large-scale fluctuations. Thermal instability can be important for the structure formation.

We sketch ISM structure formation such as molecular clouds as follows. The hot ionized ISM cools to be cold and weakly ionized clouds. Ionization degree of ISM decreases as it evolves, and then the ISM fluid is often partially ionized. In partially ionized fluid, an ion component and neutral component interact each other, exchanging the momentum (i.e., ion-neutral friction). Especially, the partially ionized plasma in a magnetic field could not be treated as one fluid. This is because although the ion component in the partially ionized plasma is directly influenced by a magnetic field, the neutral component does not directly feel a magnetic field. In weakly ionized fluid, the neutral component is affected by a magnetic field via the ion-neutral friction. For example, ambipolar diffusion takes an

important role in dynamical evolution owing to the gravitational instability of ISM into protostar (Mestel & Spitzer 1956; Nakano 1976). If the fluid frozen in a magnetic field contracts without ambipolar diffusion, the magnetic field becomes too large and suppresses the growth by the magnetic pressure and tension. In addition, Nakano (1979) points out the possibility that ISM with sufficient magnetic flux quasistatically evolves into protostar. He also notices that the time scale of plasma drift depends on the ionization degree. The relation among the ion-neutral friction, the magnetic field, and the amount of the ion component is important to understand the detailed process.

We here emphasize that the MHD approximation is not always applicable for our purpose in this paper. The thermal instability is effective in small structure formation, during which a neutral component is not always enough frozen in an ion component dynamically to be treated as one fluid. There is a possibility that the ion component can drift away owing to ambipolar diffusion, and that the system can contract owing to thermal instability. Then, in the present paper, to study how the ion-neutral drag and magnetic field influence the growth of the thermal instability, we treat the plasma as the two fluid of ions and neutrals. We assume that the ionization degree is very small, because we are interested in the final stage of the formation of a molecular cloud, in which the ionization degree decreases very much. We focus on the condensation mode of thermal instability, since it is important in structure formation, rather than the oscillation (overstable) mode. In §2, the problem is formulated. The property of the dispersion relation of the instability is presented in §3. Several discussions relating to the instability are found in §4. Applicability of our results to cold H I medium is briefly examined in §5, and then we summarize the paper in §6.

2. BASIC EQUATIONS AND DISPERSION RELATION

2.1. Basic Equations

The basic equations for ion-neutral two component fluid are as follows. The continuity equation, equation of motion, energy equation, and equation of state are

$$\frac{\partial \rho_n}{\partial t} + \nabla(\rho_n \mathbf{v}_n) = 0, \quad (1)$$

$$\rho_n \left[\frac{\partial \mathbf{v}_n}{\partial t} + (\mathbf{v}_n \cdot \nabla) \mathbf{v}_n \right] = -\nabla p_n - \rho_n \nu_{ni} (\mathbf{v}_n - \mathbf{v}_i), \quad (2)$$

$$\frac{1}{\gamma - 1} \left[\frac{\partial p_n}{\partial t} + (\mathbf{v}_n \cdot \nabla) p_n \right] - \frac{\gamma}{\gamma - 1} \frac{p_n}{\rho_n} \left[\frac{\partial \rho_n}{\partial t} + (\mathbf{v}_n \cdot \nabla) \rho_n \right] = -\rho_n \Lambda_n + \nabla(K_n \nabla T_n), \quad (3)$$

and

$$p_n = \frac{\mathcal{R}}{\mu_n} \rho_n T_n, \quad (4)$$

for a neutral component. Those for an ion component are

$$\frac{\partial \rho_i}{\partial t} + \nabla(\rho_i \mathbf{v}_i) = 0, \quad (5)$$

$$\begin{aligned} \rho_i \left[\frac{\partial \mathbf{v}_i}{\partial t} + (\mathbf{v}_i \cdot \nabla) \mathbf{v}_i \right] &= -\nabla p_i - \rho_n \nu_{ni} (\mathbf{v}_i - \mathbf{v}_n) \\ &\quad + \frac{1}{4\pi} (\nabla \times \mathbf{B}) \times \mathbf{B}, \end{aligned} \quad (6)$$

$$\frac{1}{\gamma - 1} \left[\frac{\partial p_i}{\partial t} + (\mathbf{v}_i \cdot \nabla) p_i \right] - \frac{\gamma}{\gamma - 1} \frac{p_i}{\rho_i} \left[\frac{\partial \rho_i}{\partial t} + (\mathbf{v}_i \cdot \nabla) \rho_i \right] = -\rho_i \Lambda_i + \nabla(K_i \nabla T_i), \quad (7)$$

$$p_i = \frac{\mathcal{R}}{\mu_i} \rho_i T_i, \quad (8)$$

and the induction equation is

$$\frac{\partial \mathbf{B}}{\partial t} = \nabla \times (\mathbf{v}_i \times \mathbf{B}). \quad (9)$$

Here, the subscript, n, denotes neutral, and subscript, i, does ion. Variables ρ , \mathbf{v} , p , T , and \mathbf{B} express density, velocity, pressure, temperature, and a magnetic field, respectively. The cooling function Λ is defined as energy losses minus energy gains per gram per second. In addition, the coefficient of thermal conductivity is expressed by K , the gas constant by \mathcal{R} , and the mean molecular weight by μ .

The second terms on the right-hand sides of equations (2) and (6) mean the effect of dragging through the neutral-ion collision, similarly to Watson et al. (2004). The neutral-ion collision frequency ν_{ni} is expressed as $\gamma_\nu \rho_i$, where γ_ν is the collision rate coefficient per unit mass,

$$\gamma_\nu \equiv \frac{\langle \sigma v \rangle}{m_i + m_n}. \quad (10)$$

Here, σ is the collision cross-section, v is the relative velocity between ion and neutral components, m is mass, and the angular bracket of $\langle \rangle$ expresses a mean value over all velocities. It is pointed out that the larger the friction is, the better the one fluid approximation of the partially ionized plasma is like a classical MHD approximation.

The effect of the heat flow between the two components due to the difference of the temperatures is neglected as second order terms because we assume the temperatures of two components under the equilibrium are identical. In addition, the frictional heating is also neglected as second order terms because the mutual velocity between the two components is zero in the equilibrium.

2.2. Dispersion Relation

We solve the perturbed basic equations, considering the first order. The unperturbed state is supposed to be infinite, uniform, static, and isothermal in equilibrium. It is described with subscript 0, such as $\rho_n = \rho_{n0}$, $p_n = p_{n0}$, $\mathbf{v}_n = \mathbf{v}_{n0} = 0$, $T_n = T_{n0}$, $\rho_i = \rho_{i0}$, $p_i = p_{i0}$, $\mathbf{v}_i = \mathbf{v}_{i0} = 0$, $T_i = T_{i0}$, and $\mathbf{B} = \mathbf{B}_0$. The magnetic field \mathbf{B}_0 in equilibrium can be taken as $\mathbf{B}_0 = (0, 0, B_0)$ for simplicity. The net transfer of thermal energy for each component in equilibrium is zero, such as $\Lambda_n(\rho_{n0}, T_{n0}) = 0$ and $\Lambda_i(\rho_{i0}, T_{i0}) = 0$.

Someone might think our unperturbed state is inadequate since the size of the unperturbed medium is infinite. However, in our so-called WKB framework, we can state how our unperturbed condition is useful. As long as the WKB approximation is adopted, the whole of the system should be large. This can correspond to the fact that the scale length of the galactic gas disk is about 100 pc, which is always much longer than the so-called Field length, λ_F . That is, since the interesting wave-length of the instability for the structure formation is smaller than the thickness of the galactic disk, our study is meaningful.

We take the perturbation as

$$a(\mathbf{r}, t) = a_1 \exp(nt + i\mathbf{k} \cdot \mathbf{r}), \quad (11)$$

according to Field (1965), where a_1 is the amplitude of perturbation, n is the growth rate of perturbation, and \mathbf{k} is the wave number of perturbation. When n is real and positive, the perturbation grows exponentially as a condensation mode. If n is real and negative, the perturbation damps. When n is complex number, the system is oscillatory growing or damping. Of course, when $\Re[n]$ is positive, the system is so-called overstable.

In order to know how the magnetic field affects on weakly ionized fluid, we mainly investigate the condensation mode, because we are interested in the formation and evolution of molecular clouds. We assume that

$$\mathbf{B}_0 \perp \mathbf{k} \quad \text{and} \quad \mathbf{k} \parallel \mathbf{v}_{i1} \parallel \mathbf{v}_{n1} \quad (12)$$

for comfort. Due to the induction equation (9), these assumptions lead to

$$\mathbf{B}_0 \parallel \mathbf{B}_1, \quad (13)$$

[see equation (A9) in Appendix A]. It is emphasized that the assumed magnetic field is perpendicular to the fluid motion.

Here, it is noticed that we can examine some other modes, which do not satisfy the condition (12) and (13), when $\mathbf{B}_0 = 0$. This means $\mathbf{B}_1 = 0$, owing to the induction equation

(9). In other words, we can study the property of the dispersion relation when the magnetic field does not work effectively. This is interesting point in our analysis since those modes with $\mathbf{B}_0 = 0$ yield understanding of the pure effect by the ion-neutral friction. It is also noted that there is no thermal instability in a pure Alfvén mode which satisfies $\mathbf{v} \perp \mathbf{k}$, because the Alfvén mode is effectively incompressible, and there is no net thermal exchange, even if the fluid is compressible.

In this paper, since we are interested in the structure formation from H I medium, the fluid is assumed to be weakly ionized, i.e., $\rho_{i0} \ll \rho_{n0}$. We also assume that temperatures of neutral and ion components are the same in the equilibrium, i.e., $T_{n0} = T_{i0}$, because they are well mixed and collide enough to have the same temperature for fewness of ion component. Using these conditions and replacing $|\mathbf{k}| = k$, here is the dispersion relation (see Appendix A for the derivation in detail):

$$\begin{aligned}
& \left[n^3 + n^2 \left(v_{\text{sn}} k_{\text{nT}} + v_{\text{sn}} k \frac{k}{k_{\text{nK}}} \right) + n(v_{\text{sn}} k)^2 + \frac{1}{\gamma} (v_{\text{sn}} k)^2 \left(v_{\text{sn}} k_{\text{nT}} - v_{\text{sn}} k_{\text{n}\rho} + v_{\text{sn}} k \frac{k}{k_{\text{nK}}} \right) \right] \\
& \times \left[n^3 + n^2 \left(v_{\text{si}} k_{\text{iT}} + v_{\text{si}} k \frac{k}{k_{\text{iK}}} \right) + n(v_{\text{si}} k)^2 + n(v_{\text{A}} k)^2 \right. \\
& \quad \left. + \frac{1}{\gamma} \left(v_{\text{si}} k_{\text{iT}} + v_{\text{si}} k \frac{k}{k_{\text{iK}}} \right) (v_{\text{si}}^2 k^2 + \gamma v_{\text{A}}^2 k^2) - \frac{1}{\gamma} (v_{\text{si}} k)^2 (v_{\text{si}} k_{\text{i}\rho}) \right] \\
& = -\nu_{\text{ni}0} \frac{1}{\chi} \cdot \left\{ n^5 + n^4 \left(v_{\text{si}} k_{\text{iT}} + v_{\text{si}} k \frac{k}{k_{\text{iK}}} + v_{\text{sn}} k_{\text{nT}} + v_{\text{sn}} k \frac{k}{k_{\text{nK}}} \right) \right. \\
& \quad + n^3 \left[v_{\text{sn}} k \frac{k}{k_{\text{nK}}} v_{\text{si}} k \frac{k}{k_{\text{iK}}} + v_{\text{sn}} k \frac{k}{k_{\text{nK}}} v_{\text{si}} k_{\text{iT}} + v_{\text{si}} k \frac{k}{k_{\text{iK}}} v_{\text{sn}} k_{\text{nT}} + v_{\text{sn}} k_{\text{nT}} v_{\text{si}} k_{\text{iT}} \right. \\
& \quad \left. \left. + (v_{\text{sn}} k)^2 + (v_{\text{A}} k)^2 \chi \right] \right. \\
& \quad + n^2 \left[\frac{1}{\gamma} (v_{\text{sn}} k)^2 (v_{\text{sn}} k_{\text{nT}} + v_{\text{sn}} k \frac{k}{k_{\text{nK}}}) - \frac{1}{\gamma} (v_{\text{sn}} k)^2 v_{\text{sn}} k_{\text{n}\rho} + (v_{\text{sn}} k)^2 (v_{\text{si}} k_{\text{iT}} + v_{\text{si}} k \frac{k}{k_{\text{iK}}}) \right. \\
& \quad \left. - \frac{1}{\gamma} \chi (v_{\text{si}} k)^2 v_{\text{si}} k_{\text{i}\rho} + (v_{\text{A}} k)^2 \chi \left(v_{\text{si}} k_{\text{iT}} + v_{\text{si}} k \frac{k}{k_{\text{iK}}} + v_{\text{sn}} k_{\text{nT}} + v_{\text{sn}} k \frac{k}{k_{\text{nK}}} \right) \right] \\
& \quad + n \left[(v_{\text{A}}^2 k^2 \chi + \frac{1}{\gamma} v_{\text{sn}}^2 k^2) \right. \\
& \quad \left. \left(v_{\text{sn}} k \frac{k}{k_{\text{nK}}} v_{\text{si}} k \frac{k}{k_{\text{iK}}} + v_{\text{sn}} k \frac{k}{k_{\text{nK}}} v_{\text{si}} k_{\text{iT}} + v_{\text{si}} k \frac{k}{k_{\text{iK}}} v_{\text{sn}} k_{\text{nT}} + v_{\text{sn}} k_{\text{nT}} v_{\text{si}} k_{\text{iT}} \right) \right. \\
& \quad \left. - \frac{1}{\gamma} \chi (v_{\text{si}} k)^2 v_{\text{si}} k_{\text{i}\rho} (v_{\text{sn}} k_{\text{nT}} + v_{\text{sn}} k \frac{k}{k_{\text{nK}}}) - \frac{1}{\gamma} (v_{\text{sn}} k)^2 v_{\text{sn}} k_{\text{n}\rho} (v_{\text{si}} k_{\text{iT}} + v_{\text{si}} k \frac{k}{k_{\text{iK}}}) \right] \Bigg\}, \quad (14)
\end{aligned}$$

where

$$v_{\text{sn}}^2 = \gamma \frac{p_{\text{n}0}}{\rho_{\text{n}0}}, \quad v_{\text{si}}^2 = \gamma \frac{p_{\text{i}0}}{\rho_{\text{i}0}}, \quad v_{\text{A}}^2 = \frac{B_0^2}{4\pi \rho_{\text{i}0}}, \quad (15)$$

$$k_{\text{n}\rho} = \frac{\mu_{\text{n}}(\gamma - 1)\rho_{\text{n}0}\Lambda_{\text{n}\rho}}{\mathcal{R}v_{\text{sn}}T_{\text{n}0}}, \quad k_{\text{nT}} = \frac{\mu_{\text{n}}(\gamma - 1)\Lambda_{\text{nT}}}{\mathcal{R}v_{\text{sn}}}, \quad k_{\text{nK}} = \frac{\mathcal{R}v_{\text{sn}}\rho_{\text{n}0}}{\mu_{\text{n}}(\gamma - 1)K_{\text{n}0}}, \quad (16)$$

$$k_{\text{i}\rho} = \frac{\mu_{\text{i}}(\gamma - 1)\rho_{\text{i}0}\Lambda_{\text{i}\rho}}{\mathcal{R}v_{\text{si}}T_{\text{i}0}}, \quad k_{\text{iT}} = \frac{\mu_{\text{i}}(\gamma - 1)\Lambda_{\text{iT}}}{\mathcal{R}v_{\text{si}}}, \quad k_{\text{iK}} = \frac{\mathcal{R}v_{\text{si}}\rho_{\text{i}0}}{\mu_{\text{i}}(\gamma - 1)K_{\text{i}0}}, \quad (17)$$

and

$$\nu_{\text{ni}0} \equiv \gamma_{\nu} \rho_{\text{i}0}, \quad \chi \equiv \frac{\rho_{\text{i}0}}{\rho_{\text{n}0}}. \quad (18)$$

In addition,

$$\Lambda_{\text{n}\rho} \equiv \left(\frac{\partial \Lambda_{\text{n}}}{\partial \rho_{\text{n}}} \right)_{T_{\text{n}}}, \quad \Lambda_{\text{nT}} \equiv \left(\frac{\partial \Lambda_{\text{n}}}{\partial T_{\text{n}}} \right)_{\rho_{\text{n}}}, \quad \Lambda_{\text{i}\rho} \equiv \left(\frac{\partial \Lambda_{\text{i}}}{\partial \rho_{\text{i}}} \right)_{T_{\text{i}}}, \quad \Lambda_{\text{iT}} \equiv \left(\frac{\partial \Lambda_{\text{i}}}{\partial T_{\text{i}}} \right)_{\rho_{\text{i}}}, \quad (19)$$

and they are evaluated in the equilibrium state.

The dispersion relation (14) is the equation of sixth order of n . This dispersion relation connotes the two sets of three modes. One of the three modes in each set is condensation mode, and the other two modes are oscillation modes originally, if there is no friction effect. The first bracket on the left-hand side in equation (14) is the dispersion relation of three modes of only neutral fluid (B1). The second in equation (14) is the dispersion relation of only ionized fluid in the magnetic field (B2). The right-hand side of equation (14) expresses the momentum exchange through the ion-neutral drag. The properties of the thermal instability of one fluid approximation is also briefly mentioned in Appendix B.

3. RESULTS

3.1. Critical Wavelength of the Condensation Mode

Observing the dispersion relation (14), we obtain the first result that a critical wavelength for the instability in a condensation mode is not affected by the friction. The critical wavelength is evaluated if we let n be zero, because the growth rate of n is zero at the critical wavelength. Thus, letting $n = 0$, we find the right-hand side of equation (14), which denotes the effect of the ion-neutral friction, diminishes. That is, the effect of the friction does not play any roles to determine the critical wavelength of the condensation mode. The criterion of the instability for the partially ionized plasma is estimated as if there is no friction. Although the critical wavelength is not affected, the friction affects the growth rate of the thermal instability. It is noted that the criterion of the overstability modes is not derived by the same way like the condensation mode since n is imaginary.

3.2. Growth Rate of Condensation Mode of the Instability

3.2.1. Description of the Conditions

The dispersion relation (14) is numerically solved by means of MATHEMATICA, after the normalization (see Appendix C). We study the condensation mode which is important on structure formation. To present the numerical dispersion relations, we take the following parameters : $\gamma = 5/3$, $\alpha_n \equiv k_{nT}/k_{n\rho} = 1/2$, $\alpha_i \equiv k_{iT}/k_{i\rho} = 1/2$, $\beta_n \equiv k_{n\rho}/k_{nK} = 0.01$, $\beta_i \equiv k_{i\rho}/k_{iK} = 0.01$, for the comparison to Field (1965). We set these parameters to be fixed because we are concerned for the basic nature of two-component fluid and compare the results with one-component fluid. We assume that $\mu_n = 1$, $\mu_i = 1/2$, for e.g., only H

atom plasma, $\chi = 0.01$, and $k_{i\rho} = k_{n\rho}$. Under these conditions, the dispersion relation (14) is evaluated for the various quantities of v_A/v_{sn} which corresponds to the strength of the magnetic field, and $\nu_{ni0}/(k_{n\rho}v_{sn})$ which corresponds to the strength of the friction.

Before showing the precise results of the numerical dispersion relations, we examine the physical meaning of the axis of the following figures. In each figure, the horizontal axis is the wave number k in units of $k_{n\rho}$. The vertical axis corresponds to the growth rate $\Re[n]$ in units of $k_{n\rho}v_{sn}$. These normalizations are adopted to denote the characteristic property of the thermal instability. The wavelength is taken as λ . We shall start considering the physical meaning of $k_{n\rho}$. According to equation (16) with approximation of $\rho_{n0}\Lambda_{n\rho} \sim \Lambda_n$,

$$\begin{aligned} k_{n\rho} &= \frac{\mu_n(\gamma - 1)\rho_{n0}\Lambda_{n\rho}}{\mathcal{R}v_{sn}T_{n0}} \\ &\sim \frac{\rho_{n0}\Lambda_n}{p_{n0}} \cdot \frac{1}{v_{sn}}, \end{aligned} \quad (20)$$

where $p_{n0}/\rho_{n0}\Lambda_n$ expresses the cooling time. Then, we find $k_{n\rho}^{-1}$ is interpreted as the distance for the fluid to acoustically move within the cooling time. In other words, it is interpreted as the length scale in which the fluid can respond to the perturbation. Therefore, regarding the horizontal axis, $(k/k_{n\rho})^{-1} \sim \lambda k_{n\rho}$ is interpreted as the scalelength in units where the fluid can respond to the thermal instability within the cooling time (i.e., the growing time). We get some physical intuition once the above normalization is adopted. For example, we get physical intuition when $(k/k_{n\rho})^{-1} \gg 1$, the fluid is hard to respond to the thermal instability. This is because the system is too large and the acoustic wave which carries the disturbance can not travel through the whole system within the cooling time. Then, the growth rate at $(k/k_{n\rho})^{-1} \gg 1$ is reduced down in each figure. When $(k/k_{n\rho})^{-1} < 1$, the fluid is easy to respond to the thermal instability.

Similarly, regarding the vertical axis, $\Re[n]/k_{n\rho}v_{sn}$ is interpreted as n multiplied by the cooling time. In other word, it is interpreted as the cooling time divided by the time scale for the growth of the instability. Then, the vertical axis means how fast the instability can grow up compared with the cooling time. The thermal instability is due to the cooling, then the value of $\Re[n]/k_{n\rho}v_{sn}$ should be less than unity as presented in each figure.

3.2.2. Various Conditions of the Friction and Magnetic Field

Figure 1 displays the dispersion relation of the real part of n when there exists neither the magnetic field nor friction. A dot-dashed curve corresponds to a mode characterized by μ_i and a dashed one to that of μ_n . No friction means that the motion of the ion and

neutral components are independent completely, and thus a dot-dashed curve corresponds to a single ionized fluid and a dashed one to a simple neutral fluid. The difference between the two curves comes from the mean molecular weight. This result follows Field (1965).

Figure 2 shows the growth rate when there is no magnetic field but some friction [i.e., $v_A/v_{sn} = 0$, $\nu_{ni0}/(k_{n\rho}v_{sn}) = 0.03$]. This condition yields understanding of the pure effect of the friction. When there exists the friction, a pure mode of an ion component or a neutral one does not exist. Therefore, interpretation is required on what a curve in the figure means when there exists the friction. The resultant modes with the friction are displays as two thick lines. For comparison, the two thin lines when there exists neither a magnetic field nor friction in Figure 1 are also plotted. A thick dot-dashed curve originates from an ion component mode of Figure 1. A thick dashed curve originates from an neutral component of Figure 1. These interpretations are reasonable since the effect of mean molecular weight of each component is imprinted in each dispersion relation. The difference between the Figure 1 and 2 is that the growth rate at the larger scale decreases, compared with the original modes of Figure 1. This is because the suppression by the friction is more efficient at rather larger scale. The longer distance particles move, the more frequent the collision from which the friction originates is. It is noticed that the current model corresponds to the case that the fluid moves along the field line if there exists the magnetic field. Figure 2 shows that only the friction suppresses the instability along the field line, while the magnetic field does not.

Figure 3 shows the growth rate when the friction is the same as Figure 2, but there is the finite magnetic field [i.e., $v_A/v_{sn} = 0.6$, $\nu_{ni0}/(k_{n\rho}v_{sn}) = 0.03$]. For comparison, the two thin curves which correspond to the results of Figure 1 are also displayed, as well as Figure 2. A thick dashed curve is a mode, which is characterized by μ_i . The reason why the curve is interpreted to relating to μ_i is that the critical wavelength is enlarged owing to the stabilization of the magnetic field [see the criterion (B2)]. That is, the magnetic field suppresses a kind of mode of the thermal instability. A thick dot-dashed curve is characterized by μ_n . The critical wavelength of this mode is not affected by the magnetic field. Thus, the mode characterized by μ_n is hardly affected by the field. This occurs since the amount of the neutral component significantly dominates that of the ion component.

Figure 4 shows the growth rate when the magnetic field is thousand times of that in Figure 3, and friction is ten times of that in Figure 3 [i.e., $v_A/v_{sn} = 600$, $\nu_{ni0}/(k_{n\rho}v_{sn}) = 0.3$]. The large magnetic field completely stabilizes a mode characterized by μ_i so that this mode does not appear in this figure. Thus, there is displayed only one mode of the thermal instability characterized by μ_n . This is expressed by the thick dot-dashed curve. For comparison, the two thin curves are displayed as well as Figure 2. Figure 5 shows the

growth rate when the magnetic field is ten times of that in Figure 4 and friction is the same as in Figure 4 [i.e., $v_A/v_{sn} = 6000$, $\nu_{ni0}/(k_{n\rho}v_{sn}) = 0.3$]. The large magnetic field completely stabilizes a mode characterized by μ_i . The thick dot-dashed curve expresses the mode of thermal instability characterized by μ_n . For comparison, the two thin curves are displayed as well as Figure 2. It is noted that Figures 4 and 5 show that the suppression by the magnetic field is saturated (see subsection 4.3).

In Figure 6, the friction is stronger than that in Figure 4, but the magnetic field is the same [i.e., $v_A/v_{sn} = 600$, $\nu_{ni0}/(k_{n\rho}v_{sn}) = 5$]. For comparison, the two thin curves are displayed like Figure 2. A mode characterized by μ_i is completely stabilized, and then it disappears here. A mode characterized by μ_n is still unstable, while the growth rate is reduced. That is, even in weakly ionized fluid, the growth of the thermal instability is affected by the magnetic field through the friction. This decrement of the growth rate is significant at longer scale. We also confirm that the characteristic wavelength at the maximum growth rate of the instability shifts shortward as the growth rate diminishes. This occurs since the friction is effective at larger scale and the conduction is effective at smaller scale, so that the growth rate at larger scale decreases significantly. Then, the characteristic wavelength at the maximum growth rate becomes small.

It should be emphasized that all the critical wavelengths of the unstable mode characterized by μ_n are equivalent among Figures 1 – 6. The frictional terms in the right hand side of the dispersion relation (14) are independent of the critical wavelength for the condensation mode, as mentioned in subsection 3.1. The critical wavelength of the mode relating μ_n is not changed by the magnetic field with the friction as long as the thermal conduction is not changed by the magnetic field. This point is investigated more in the following subsection 4.1.

4. DISCUSSION

We study the basic property of the thermal instability of the weakly ionized plasma in the previous sections. In this section, basing on our understanding the thermal instability, we shall discuss the structure formation.

4.1. Critical Wavelength and Thermal Conduction

First in this section, the critical wavelength of the weakly ionized plasma in the magnetic field is discussed. As mentioned in section 3, the critical wavelength of the mode relating μ_n

is not changed by the magnetic field with the friction as long as the thermal conduction is not changed by the magnetic field. In fact, the thermal conductivity is varied owing to the magnetic field. In this meaning, we may oversimplify the problem in this paper.

However, the thermal conductivity will decrease as the magnetic field strength increases, and then the critical length become smaller, according to equation (B4). Thermal conduction erases the temperature perturbation and thermally stabilizes the system, especially at smaller scale. The larger thermal conduction makes the critical wavelength longer, owing to the criterion B1 or B2, according to Field (1965). On the other hand, the magnetic field lessens the thermal conduction of the ion component, because the ion component winds around a magnetic field.

Therefore, we can insist that the critical length for the thermal instability of the weakly ionized plasma can not be enlarged by the friction and the magnetic field at least, while the effect of the magnetic field can influence not only the ion but the neutral component via the ion-neutral friction. This statement has universal validity for the thermal instability of the weakly ionized plasma. The effect of the friction and the magnetic field is mainly reduction of the growth rate of the thermal instability. On the other hand, the magnetic field directly enlarges the critical wavelength of the mode characterized by μ_i as expected in the one fluid plasma model.

4.2. Spatial Distribution of Magnetized Interstellar Medium

In the previous section, we learn that the suppression of the thermal instability is characterized by the ion-neutral friction, strength of the magnetic field, and the direction of the field. Interestingly, the suppression of the instability is different owing to the magnetic field direction. This suggests the anisotropic nature of the suppression of the instability is imprinted in the morphology of the structure. In this standing point, we shall discuss how the structure formation proceeds in the magnetized ISM.

4.2.1. Growth Rate Parallel to the Magnetic Field

In an usual one fluid approach, the motion of the plasma parallel to the magnetic field is regarded not to be affected. However, Figure 2 suggests that the growth rate of the thermal instability at larger scale decreases via the ion-neutral friction. This suppression of the instability yields the delay of the evolution in comparison to the evolution under the MHD approximation without the ion-neutral friction.

4.2.2. *Distribution of Partially Ionized Plasma Perpendicular to the Magnetic Field Line*

Here, we suggest that the spatial distribution of the partially ionized plasma is elongated, whose semi-major axis is vertical to the magnetic field line. Figures 2 and 3, both of which friction strengths are the same, show the feasibility. The thermal instability in Figure 2 corresponds to the mode along the magnetic field line since $\mathbf{B} = 0$, while that in Figure 3 is vertical to the magnetic field line. The growth of thermal instability vertical to the line is suppressed by both of the magnetic field and the friction, while the growth along the line is suppressed only by the friction. Thus, the growth rate along the magnetic field line is larger than that vertical to the line, and then the resultant morphology of the structure via the thermal instability is elongated.

4.2.3. *Difference of Spatial Distribution of Ion and Neutral Components*

We insist the growth rate depending on the direction of the field results in the morphology of interstellar structure. Furthermore, we learn in §3 the mode characterized by μ_i are stabilized by the friction and field, while that by μ_n can grow as found in Figure 3. Figure 6 shows that although the mode characterized by μ_i is completely stabilized, the mode characterized by μ_n is still unstable. Consequently, we can insist that the neutral component condenses owing to the thermal instability, while the ion component still keeps spreading.

It is noticed that the ion component may condense since it is dragged by the neutral component contracting owing to the thermal instability. However, once the distribution of the ion and the neutral components separates and the motion of the two becomes independent there, the ion component in the area is thermally stable owing to the magnetic field. This means the magnetic pressure lets the ion component be spread in the area even if the neutral component condenses.

This thin ion component left behind by the contracting neutral component will be observed as a halo around H I clouds, and it emits, especially some forbidden lines. This halo possibly has wide distribution vertical to the magnetic field, as discussed in subsection 4.2.2. This is because the ion component can condense, parallel to the magnetic field like the neutral. The magnetic pressure can not prevent the motion of the ion component efficiently as found in Figure 2. Thus, the morphology of the ion halo is also elongated according to the orientation of the field line.

4.2.4. *Origin of the Small Clumpinesses of Partially Ionized Plasma*

It is suggested that there are small clumpy structures of ISM. Here, we examine whether the clumpiness originates via the thermal instability. According to Figures 4 and 6, the growth rate of the thermal instability of partially ionized plasma depends on the strength of the friction. The scale length at the maximum growth rate of the instability becomes smaller, owing to the suppression via the friction which is effective at larger scale. Thus, we can expect the small clumpiness appears selectively via the thermal instability since the ion-neutral friction suppresses the large scale condensations.

If we are interested in the small clumpiness of ISM, we should mention about the thermal conduction in relation to the magnetic field. According to subsection 4.1, the small clumpiness may be the results of the decrement of the conduction. It is noticed that the conduction along the field line is not so affected, and then there is still ambiguity for the reduced conduction coefficient to perform the key role for the origin of the small clumpiness.

It is also noticed that the thermal instability is a slow process relative to the dynamical processes. If molecular clouds form from the H I medium via the gravitational instability, the small clumpiness inside the molecular clouds appears after the formation of the clouds. This trend is enhanced if the effects of the magnetic field and friction are concerned. This is because the friction and the field suppress the large scale growth, while the short wavelength modes are still unstable. In a enough long span for the growth, the tiny structures can appear in ISM and affect the evolution of its structure especially as the non-linear effects. Thus, if we want to know how faint and small structures come to be observable, the growth time-scale of the thermal instability should be precisely examined. At this time, we never forget the effect of the magnetic field and the ion-neutral friction.

4.3. **Ineffectiveness of the Magnetic Field**

The modes in Figures 4 and 5 have similar growth rate, while the magnetic fields are significantly different in each other. It implies that the suppression of the growth by increasing the magnetic field with the fixed friction has limits. By the way, a dispersion relation of only ionized fluid in a magnetic field, which is derived by equalizing the second bracket on the left-hand side in equation (14) to be zero, is reduced to

$$n^3 + n^2 v_{\text{si}} k_{\text{iT}} = 0, \quad (21)$$

when k approaches 0. This is solved to be

$$n = 0 \text{ or } n = -v_{\text{si}} k_{\text{iT}}. \quad (22)$$

Thus, we find that this solution is independent of a magnetic field. Even if the magnetic field becomes strong, the value of the growth rate at $k \sim 0$ is scarcely changed, where the friction is more effective than at small wavelength. Therefore, once the effect of the friction is fixed, increasing the magnetic field strength beyond a threshold level apparently becomes ineffective for the suppression of the growth. Not only information of the magnetic field but the friction is necessary to investigate the evolution of the thermal instability of the weakly ionized plasma.

4.4. Comment on One Fluid Approximation

The formulation of the fully one component plasma can not be always applicable to study the thermal instability of weakly ionized plasma. This is because there is the growing mode even when there exist the magnetic field and friction, whose growth rate is comparable to that of the neutral component when there are no magnetic field and friction. Indeed, this trend is found from the comparison among Figures 3, 4 and 5.

In addition, regarding weakly ionized plasma including the friction effect, the friction does not change the critical wavelength λ_F . The friction tends to efficiently reduce the growth at much larger scale than the λ_F . This feature yields that the critical wavelength in the weakly ionized plasma is not changed by the magnetic field via the friction, as mentioned in section 3 and subsection 4.1. Even if the magnetic field becomes strong, only the growth rate is reduced, keeping the critical wavelength constant. This is also the difference from the simple analysis of the one component magnetized plasma. The previous study of the one component plasma shows the stabilization at the smaller scales, while the current study insist λ_F is unchanged even if the effect of the field is concerned.

5. Application to Typical H I Region

In this section, we shall study the origin of the small scale structure of H I cloud as an example. The thermal instability of the typical H I region with C II cooling is briefly discussed here.

5.1. Assumptions

We assume that the temperature of H I is 100 K. The fluid mainly consists of H atom, and then $\mu_n = 1$, $\mu_i = 1/2$. We assume that $K = 4.9 \times 10^3 \text{ erg cm}^{-1} \text{ s}^{-1} \text{ K}^{-1}$, consulting the

result of Ulmschneider (1970) as thermal conductivity. In addition, we adopt the collision cross-section as $\langle\sigma v\rangle = 2 \times 10^{-9} \text{ cm}^3 \text{ s}^{-1}$ for the typical friction value according to Nakano (1976). We assume that interstellar pressure is about $10^{-12} \text{ erg cm}^{-3}$. Then, if the ISM is in equilibrium under the pressure of $10^{-12} \text{ erg cm}^{-3}$, the number density of the neutral component n_{neutral} and the magnetic field strength B are about 71.9 cm^{-3} and about 10^{-6} Gauss, respectively. The adiabatic γ is assumed to be $5/3$.

According to Wolfire et al. (1995, Fig. 3 (b)), C II cooling is dominant when $T = 100$ K. Then we adopt the expression for the C II cooling according to Wolfire et al. (1995, their Appendix B). Assuming that the fluid consists of H atom, whose mass is expressed as m_H , the cooling function Λ is

$$\Lambda = \frac{1}{m_H} \cdot 2.54 \times 10^{-14} A_C f_{\text{CII}} \cdot [\gamma^{\text{H}^0} n_{\text{H}^0} + \gamma^e n_e] \cdot \exp\left[-\frac{92}{T}\right] \text{ ergs s}^{-1} \text{ g}^{-1}. \quad (23)$$

Here, n_X is the density of element X. γ^{H^0} and γ^e are the collisional de-excitation rate coefficients of C II with neutral hydrogen and electrons, respectively. The constant f_{CII} is the fraction of C I in C II. A_C is the relative abundance of element C, defined as n_C/n . n is the density of hydrogen nuclei, defined as $n = n_{\text{H}^+} + n_{\text{H}^0}$. According to Wolfire et al. (1995),

$$\gamma^{\text{H}^0} = 8.86 \times 10^{-10} \text{ cm}^3 \text{ s}^{-1}, \quad (24)$$

$$\gamma^e = 2.1 \times 10^{-7} \left(\frac{T}{10^2}\right)^{-0.5} \left[1.80 + 0.484 \left(\frac{T}{10^4}\right) + 4.01 \left(\frac{T}{10^4}\right)^2 - 3.39 \left(\frac{T}{10^4}\right)^3\right], \quad (25)$$

and $A_C = 3 \times 10^{-4}$.

The ionization degree and the fraction of C I in C II, i.e., f_{CII} are ambiguous. Then, the ionization degree χ and the constant f_{CII} are hypothesized in some cases. We shall investigate the instability when $f_{\text{CII}} = 10^{-2}$ and $f_{\text{CII}} = 10^{-4}$. The more the amount of C II increases, the more efficient the cooling becomes. The ionization degree χ is assumed to be 10^{-6} according to the results around $n_{\text{H}} \sim 100 \text{ cm}^{-3}$ by Kamaya & Nishi (2000, Fig.1). We also investigate the instability on the extreme case when $\chi = 10^{-2}$. In addition, we assume that $\Lambda_{n\rho} = \Lambda_{i\rho}$, $\Lambda_{nT} = \Lambda_{iT}$, and $K_{n0} = K_{i0}$. This is because the ionization degree is very small and the mixing of the neutral and the ion components is sufficient. Then the temperatures T_n for the neutral and T_i for the ion become equivalent much faster than the cooling time. For example, if the temperature of the system changes by ΔT during the slight time Δt , the energy changes for the neutral and the ion are expressed as,

$$n_n k_B \Delta T \sim \rho_n \Lambda_n \Delta t$$

and

$$n_i k_B \Delta T \sim \rho_i \Lambda_i \Delta t.$$

From these equations,

$$\frac{\rho_n}{n_n}\Lambda_n \sim \frac{\rho_i}{n_i}\Lambda_i.$$

Therefore, owing to $m_n \sim m_i$ for H atoms, it is derived that $\Lambda_n \sim \Lambda_i$.

5.2. Results and Implications

Figure 7 shows the growth rate of the thermal instability when $\chi = 10^{-6}$ and $f_{\text{CII}} = 10^{-2}$. The critical wavelength for the instability is estimated to be about 0.0135 pc owing to the criterion (B1). It is noted that $\alpha_n = 0.920$, $\alpha_i = 920000$, $\beta_n = 2.19 \cdot 10^{-6}$, $\beta_i = 2.73 \cdot 10^{-7}$, $\kappa_{v_A} = 219$, $C_\nu = 0.775$, $\kappa_\rho = \chi/\mu_{\text{ni}}^2 = 5 \cdot 10^{-7}$, according to our notation summarized in Appendix C. Figure 8 shows the growth rate when $\chi = 10^{-6}$ and $f_{\text{CII}} = 10^{-4}$. The critical wavelength for the instability is estimated to be about 0.135 pc owing to the criterion (B1). Here, $\alpha_n = 0.920$, $\alpha_i = 920000$, $\beta_n = 2.19 \cdot 10^{-8}$, $\beta_i = 2.73 \cdot 10^{-9}$, $\kappa_{v_A} = 219$, $C_\nu = 77.5$, $\kappa_\rho = \chi/\mu_{\text{ni}}^2 = 5 \cdot 10^{-7}$. Figure 9 shows the growth rate when $\chi = 10^{-2}$ and $f_{\text{CII}} = 10^{-2}$. The critical wavelength for the instability is estimated to be about 0.00239 pc owing to the criterion (B1). We adopt $\alpha_n = 0.517$, $\alpha_i = 51.7$, $\beta_n = 1.15 \cdot 10^{-5}$, $\beta_i = 1.44 \cdot 10^{-6}$, $\kappa_{v_A} = 2.19$, $C_\nu = 1470$, $\kappa_\rho = \chi/\mu_{\text{ni}}^2 = 5 \cdot 10^{-3}$. To understand more, in each set of these figures, the growth rates of the following three cases are also plotted: (1) the magnetic field is hundred times as the typical value, (2) the friction is hundred times as the typical value, and (3) both of the magnetic field and the friction are hundred times as the typical value. It is noticed that the value of the horizontal and the vertical axes is normalized by $k_{n\rho}$, which is proportional to f_{CII} . The more C II (i.e., f_{CII}) increases, the shorter the critical wavelength becomes and the more the growth rate increases.

The each panel (b) in Figures 7, 8, and 9 shows characteristic results. In these panels, we find some characteristic feature of the example. At larger wavenumber than k_{max} , which corresponds to the maximum growth rate, the instability grows up as if there is no friction and field. We insist that the critical wavelengths of these cases are not enlarged because the neutral component does not suffer the effect of the magnetic field directly. At smaller wavenumber than k_{max} , the growth rate is reduced significantly. That is, the growth of the instability in the significantly large-scale is suppressed. This may indicate the quasi-static evolution like the gravitational contraction via the so-called ambipolar diffusion, if the condensation due to the thermal instability is balanced by the magnetic field via the friction.

Except the cases of $\chi = 10^{-2}$, the overall trend of the results is the same as mentioned in section 3. The instability in the very low ionization degree cases of $\chi = 10^{-6}$ is hardly

suppressed. In Figures 7 and 8, the growth at only the large scale can be suppressed by the even large friction and magnetic field. In the case of $\chi = 10^{-2}$ (Figure 9), the ionization degree is higher than the other cases, then the ion-neutral friction is more efficient. The growth rate in the panel (d) of Figure 9 is reduced all over wavelength because of the large friction. The growth of the mode in the panel (e) in Figure 9 is extremely suppressed all over the wavelength because of the large friction and the magnetic field. Especially, the growth rate at the significantly large scale (i.e., near the origin of wavenumber) approaches to the zero owing to the friction. This figure shows the possibility that the thermal instability is suppressed as well as in Figure 6. The magnetic field can become strong for the ion component to be frozen in, and the friction between the ion and the neutral components can be strong even for the high density, which are expected at the final stage of the formation.

It is noticed that under the conditions adopted in this section, the neutral component can always satisfy the thermal instability criterion, while the ion component does not satisfy the criterion. Importantly, the ionization degree is very small and then the ion component is too rare although the cooling owing to the ion component is effective for the thermal instability. Then, the thermal instability of the partially ionized plasma can not be suppressed except for the extreme case such as in the panel (e) of Figure 9. The partially ionized plasma can start to contract via the thermal instability in typical H I region, even when there exists a magnetic field. Even if the magnetic field becomes large, the growth rate is hardly suppressed except for the extreme case.

6. SUMMARY

The thermal instability of the weakly ionized fluid is investigated with a linear perturbation analysis. The plasma is assumed to consist of two fluids of the ion and the neutral components. With this approach, the effect of the friction between the ion and the neutral components and the magnetic field are important. Here, the properties of the thermal instability of weakly ionized plasma and the observational implications are summarized.

1. Modes relating to μ_n are not stabilized by the magnetic field. This is because the neutral component feels the field via the ion-neutral friction.
2. Modes relating to μ_i are directly stabilized by the magnetic field. This means that when the magnetic field is large, the ion component is hard to follow the motion of the neutrals which condensate owing to the thermal instability.
3. The growth rate of the mode vertical to the magnetic field is reduced by the magnetic field and the ion-neutral friction.

4. The growth rate of the mode along the magnetic field decreases owing to the ion-neutral friction, especially at large scale. The suppression of the instability is more ineffective than that of the mode vertical to the magnetic field.
5. The critical wavelength for the thermal instability is not affected by the friction. The effect owing to the two fluid approximation is the reduction of the growth rate of the thermal instability. The magnetic field makes the critical wavelength of modes relating μ_i larger.
6. To study the thermal instability of the partially ionized plasma, one fluid approximation is not always useful.
7. The ion-neutral friction and the magnetic field affect the distribution or morphology of ISM, especially after the long time compared to the free-fall time. The difference between the growth rate along and perpendicular to the magnetic field is important. The partially ionized plasma possibly is elongated perpendicular to the magnetic field. In addition, the neutral component and the ion component of weakly ionized fluid in the magnetic field are possibly separated each other. Then, the neutral component condenses owing to thermal instability, while the ion component left behind by the contracting neutral component still keeps spreading. Therefore, it is possibly observed that the weakly ionized fluid is elongated vertically to the magnetic field and surrounded by a halo which is rare and diffuse ions and emits forbidden lines.

To conclude, the treating both of the independent motions of the neutral and the ion components yield the ion-neutral friction. The friction is important for the thermal instability of weakly ionized fluid, especially when studying the structure formation such as molecular cloud at its final stage of formation. Our study indicates that the fully ionized plasma approximation or totally neutral fluid approximation is not always applicable to weakly ionized plasma.

We would like to thank the referee for constructive comments. We would like to thank Hiroshi Koyama for useful discussions. We would like to thank Tsuyoshi Inoue for useful comments. We would like to thank Jun Fukue for useful comments and encouragements. We would like to thank Tetsuya Nagata for encouragements and helps. Tsubasa Fukue is supported by Research Fellowships of the Japan Society for the Promotion of Science for Young Scientists. This work was partially supported by KAKENHI 18-3219. This work is partially supported by the Grant-in-Aid for the 21st Century COE "Center for Diversity and Universality in Physics" from the Ministry of Education, Culture, Sports, Science and Technology (MEXT) of Japan.

Appendix

A. Derivation of the Dispersion Relation by Linear Perturbation Analysis

We derive the dispersion relation (14) in this Appendix. We adopt the perturbations as equation (11), that is, $a(\mathbf{r}, t) = a_1 \exp(nt + i\mathbf{k} \cdot \mathbf{r})$. Basic equations (1)–(9) are then linearized as follows:

$$\rho_{n1}n + i\rho_{n0}\mathbf{v}_{n1} \cdot \mathbf{k} = 0, \quad (\text{A1})$$

$$n\rho_{n0}\mathbf{v}_{n1} = -p_{n1}i\mathbf{k} - \rho_{n0}\nu_{ni}(\mathbf{v}_{n1} - \mathbf{v}_{i1}), \quad (\text{A2})$$

$$\frac{1}{\gamma - 1}p_{n1}n - \frac{\gamma}{\gamma - 1}\frac{p_{n0}}{\rho_{n0}}n\rho_{n1} = -\rho_{n0}(\rho_{n1}\Lambda_{n\rho} + T_{n1}\Lambda_{nT}) - K_{n0}T_{n1}k^2, \quad (\text{A3})$$

$$\frac{p_{n1}}{p_{n0}} = \frac{\rho_{n1}}{\rho_{n0}} + \frac{T_{n1}}{T_{n0}}, \quad (\text{A4})$$

$$\rho_{i1}n + i\rho_{i0}\mathbf{v}_{i1} \cdot \mathbf{k} = 0, \quad (\text{A5})$$

$$n\rho_{i0}\mathbf{v}_{i1} = -p_{i1}i\mathbf{k} - \rho_{i0}\nu_{ni}(\mathbf{v}_{i1} - \mathbf{v}_{n1}) + \frac{1}{4\pi}i(\mathbf{k} \times \mathbf{B}_1) \times \mathbf{B}_0, \quad (\text{A6})$$

$$\frac{1}{\gamma - 1}p_{i1}n - \frac{\gamma}{\gamma - 1}\frac{p_{i0}}{\rho_{i0}}n\rho_{i1} = -\rho_{i0}(\rho_{i1}\Lambda_{i\rho} + T_{i1}\Lambda_{iT}) - K_{i0}T_{i1}k^2, \quad (\text{A7})$$

$$\frac{p_{i1}}{p_{i0}} = \frac{\rho_{i1}}{\rho_{i0}} + \frac{T_{i1}}{T_{i0}}, \quad (\text{A8})$$

and

$$n\mathbf{B}_1 = i[\mathbf{v}_{i1}(\mathbf{B}_0 \cdot \mathbf{k}) - \mathbf{B}_0(\mathbf{v}_{i1} \cdot \mathbf{k})]. \quad (\text{A9})$$

Using conditions $\mathbf{B}_0 \perp \mathbf{k}$, $\mathbf{k} \parallel \mathbf{v}_{i1}$, $\mathbf{k} \parallel \mathbf{v}_{n1}$, and $\mathbf{B}_0 \parallel \mathbf{B}_1$, this multi-dimensional issue is reduced to one dimensional issue. Then, vanishing of the determinant of coefficients, a dispersion relation for partially ionized plasma is derived as follows:

$$\begin{aligned}
& \left[n^3 + n^2 \left(v_{\text{sn}} k_{\text{nT}} + v_{\text{sn}} k \frac{k}{k_{\text{nK}}} \right) + n(v_{\text{sn}} k)^2 + \frac{1}{\gamma} (v_{\text{sn}} k)^2 \left(v_{\text{sn}} k_{\text{nT}} - v_{\text{sn}} k_{\text{n}\rho} + v_{\text{sn}} k \frac{k}{k_{\text{nK}}} \right) \right] \\
& \times \left[n^3 + n^2 \left(v_{\text{si}} k_{\text{iT}} + v_{\text{si}} k \frac{k}{k_{\text{iK}}} \right) + n(v_{\text{si}} k)^2 + n(v_{\text{A}} k)^2 \right. \\
& \quad \left. + \frac{1}{\gamma} \left(v_{\text{si}} k_{\text{iT}} + v_{\text{si}} k \frac{k}{k_{\text{iK}}} \right) (v_{\text{si}}^2 k^2 + \gamma v_{\text{A}}^2 k^2) - \frac{1}{\gamma} (v_{\text{si}} k)^2 (v_{\text{si}} k_{\text{i}\rho}) \right] \\
& = -\nu_{\text{ni0}} \frac{\rho_{\text{i0}} + \rho_{\text{n0}}}{\rho_{\text{i0}}} \cdot \left\{ n^5 + n^4 \left(v_{\text{si}} k_{\text{iT}} + v_{\text{si}} k \frac{k}{k_{\text{iK}}} + v_{\text{sn}} k_{\text{nT}} + v_{\text{sn}} k \frac{k}{k_{\text{nK}}} \right) \right. \\
& \quad + n^3 \left[v_{\text{sn}} k \frac{k}{k_{\text{nK}}} v_{\text{si}} k \frac{k}{k_{\text{iK}}} + v_{\text{sn}} k \frac{k}{k_{\text{nK}}} v_{\text{si}} k_{\text{iT}} + v_{\text{si}} k \frac{k}{k_{\text{iK}}} v_{\text{sn}} k_{\text{nT}} \right. \\
& \quad \left. \left. + v_{\text{sn}} k_{\text{nT}} v_{\text{si}} k_{\text{iT}} + k^2 \left(\gamma \frac{p_{\text{i0}} + p_{\text{n0}}}{\rho_{\text{i0}} + \rho_{\text{n0}}} + \frac{B_0^2}{4\pi} \frac{1}{\rho_{\text{i0}} + \rho_{\text{n0}}} \right) \right] \right. \\
& \quad + n^2 \left[\frac{p_{\text{n0}} + p_{\text{i0}} \gamma}{\rho_{\text{i0}} + \rho_{\text{n0}}} k^2 (v_{\text{sn}} k_{\text{nT}} + v_{\text{sn}} k \frac{k}{k_{\text{nK}}}) - \frac{p_{\text{n0}}}{\rho_{\text{i0}} + \rho_{\text{n0}}} k^2 v_{\text{sn}} k_{\text{n}\rho} \right. \\
& \quad + \frac{p_{\text{i0}} + p_{\text{n0}} \gamma}{\rho_{\text{i0}} + \rho_{\text{n0}}} k^2 (v_{\text{si}} k_{\text{iT}} + v_{\text{si}} k \frac{k}{k_{\text{iK}}}) - \frac{p_{\text{i0}}}{\rho_{\text{i0}} + \rho_{\text{n0}}} k^2 v_{\text{si}} k_{\text{i}\rho} \\
& \quad \left. \left. + \frac{B_0^2}{4\pi} \frac{1}{\rho_{\text{i0}} + \rho_{\text{n0}}} \left(v_{\text{si}} k_{\text{iT}} + v_{\text{si}} k \frac{k}{k_{\text{iK}}} + v_{\text{sn}} k_{\text{nT}} + v_{\text{sn}} k \frac{k}{k_{\text{nK}}} \right) \right] \right. \\
& \quad + n \left[\left(\frac{B_0^2}{4\pi} \frac{1}{\rho_{\text{i0}} + \rho_{\text{n0}}} k^2 + \frac{p_{\text{i0}} + p_{\text{n0}}}{\rho_{\text{i0}} + \rho_{\text{n0}}} k^2 \right) \right. \\
& \quad \cdot \left(v_{\text{sn}} k \frac{k}{k_{\text{nK}}} v_{\text{si}} k \frac{k}{k_{\text{iK}}} + v_{\text{sn}} k \frac{k}{k_{\text{nK}}} v_{\text{si}} k_{\text{iT}} + v_{\text{si}} k \frac{k}{k_{\text{iK}}} v_{\text{sn}} k_{\text{nT}} + v_{\text{sn}} k_{\text{nT}} v_{\text{si}} k_{\text{iT}} \right) \\
& \quad - \frac{p_{\text{i0}}}{\rho_{\text{i0}} + \rho_{\text{n0}}} k^2 v_{\text{si}} k_{\text{i}\rho} (v_{\text{sn}} k_{\text{nT}} + v_{\text{sn}} k \frac{k}{k_{\text{nK}}}) \\
& \quad \left. \left. - \frac{p_{\text{n0}}}{\rho_{\text{i0}} + \rho_{\text{n0}}} k^2 v_{\text{sn}} k_{\text{n}\rho} (v_{\text{si}} k_{\text{iT}} + v_{\text{si}} k \frac{k}{k_{\text{iK}}}) \right] \right\}. \tag{A10}
\end{aligned}$$

We emphasize that this dispersion relation is not yet assumed to be weakly ionized plasma, such as $\rho_{\text{i0}} \ll \rho_{\text{n0}}$. Here are

$$v_{\text{sn}}^2 = \gamma \frac{p_{\text{n0}}}{\rho_{\text{n0}}}, \quad v_{\text{si}}^2 = \gamma \frac{p_{\text{i0}}}{\rho_{\text{i0}}}, \quad v_{\text{A}}^2 = \frac{B_0^2}{4\pi \rho_{\text{i0}}},$$

$$k_{\text{n}\rho} = \frac{\mu_{\text{n}}(\gamma - 1)\rho_{\text{n0}}\Lambda_{\text{n}\rho}}{\mathcal{R}v_{\text{sn}}T_{\text{n0}}}, \quad k_{\text{nT}} = \frac{\mu_{\text{n}}(\gamma - 1)\Lambda_{\text{nT}}}{\mathcal{R}v_{\text{sn}}}, \quad k_{\text{nK}} = \frac{\mathcal{R}v_{\text{sn}}\rho_{\text{n0}}}{\mu_{\text{n}}(\gamma - 1)K_{\text{n0}}},$$

$$k_{\text{i}\rho} = \frac{\mu_{\text{i}}(\gamma - 1)\rho_{\text{i0}}\Lambda_{\text{i}\rho}}{\mathcal{R}v_{\text{si}}T_{\text{i0}}}, \quad k_{\text{iT}} = \frac{\mu_{\text{i}}(\gamma - 1)\Lambda_{\text{iT}}}{\mathcal{R}v_{\text{si}}}, \quad k_{\text{iK}} = \frac{\mathcal{R}v_{\text{si}}\rho_{\text{i0}}}{\mu_{\text{i}}(\gamma - 1)K_{\text{i0}}},$$

$$\Lambda_{n\rho} \equiv \left(\frac{\partial \Lambda_n}{\partial \rho_n} \right)_{T_n}, \quad \Lambda_{nT} \equiv \left(\frac{\partial \Lambda_n}{\partial T_n} \right)_{\rho_n}, \quad \Lambda_{i\rho} \equiv \left(\frac{\partial \Lambda_i}{\partial \rho_i} \right)_{T_i}, \quad \Lambda_{iT} \equiv \left(\frac{\partial \Lambda_i}{\partial T_i} \right)_{\rho_i},$$

and

$$\nu_{ni0} \equiv \gamma_\nu \rho_{i0}.$$

We assume that the fluid is weakly ionized (i.e., $\rho_{i0} \ll \rho_{n0}$) and that temperatures of neutral and ion components are the same in the equilibrium (i.e., $T_{n0} = T_{i0}$). According to $p = \mathcal{R}\rho T/\mu$, assumptions $\rho_{i0} \ll \rho_{n0}$ and $T_{n0} = T_{i0}$ lead to $p_{i0} \ll p_{n0}$. Using these approximations and the definition $\chi \equiv \rho_{i0}/\rho_{n0}$, we can replace several expressions as follows:

$$\begin{aligned} \frac{\rho_{i0} + \rho_{n0}}{\rho_{i0}} &\sim \frac{1}{\chi}, \\ \frac{p_{n0}}{\rho_{i0} + \rho_{n0}} &\sim \frac{v_{sn}^2}{\gamma}, \\ \frac{p_{i0}}{\rho_{i0} + \rho_{n0}} &\sim \frac{v_{si}^2 \chi}{\gamma}, \\ \gamma \frac{p_{i0} + p_{n0}}{\rho_{i0} + \rho_{n0}} &\sim v_{sn}^2, \\ \frac{p_{n0} + p_{i0} \gamma}{\rho_{i0} + \rho_{n0}} &\sim \frac{v_{sn}^2}{\gamma}, \\ \frac{p_{i0} + p_{n0} \gamma}{\rho_{i0} + \rho_{n0}} &\sim v_{sn}^2, \end{aligned}$$

and

$$\frac{B_0^2}{4\pi} \frac{1}{\rho_{i0} + \rho_{n0}} \sim v_A^2 \chi.$$

Then, the dispersion relation (A10) is approximated to be

$$\begin{aligned}
& \left[n^3 + n^2 \left(v_{\text{sn}} k_{\text{nT}} + v_{\text{sn}} k \frac{k}{k_{\text{nK}}} \right) + n(v_{\text{sn}} k)^2 + \frac{1}{\gamma} (v_{\text{sn}} k)^2 \left(v_{\text{sn}} k_{\text{nT}} - v_{\text{sn}} k_{\text{n}\rho} + v_{\text{sn}} k \frac{k}{k_{\text{nK}}} \right) \right] \\
& \times \left[n^3 + n^2 \left(v_{\text{si}} k_{\text{iT}} + v_{\text{si}} k \frac{k}{k_{\text{iK}}} \right) + n(v_{\text{si}} k)^2 + n(v_{\text{A}} k)^2 \right. \\
& \quad \left. + \frac{1}{\gamma} \left(v_{\text{si}} k_{\text{iT}} + v_{\text{si}} k \frac{k}{k_{\text{iK}}} \right) (v_{\text{si}}^2 k^2 + \gamma v_{\text{A}}^2 k^2) - \frac{1}{\gamma} (v_{\text{si}} k)^2 (v_{\text{si}} k_{\text{i}\rho}) \right] \\
& = -\nu_{\text{ni}0} \frac{1}{\chi} \cdot \left\{ n^5 + n^4 \left(v_{\text{si}} k_{\text{iT}} + v_{\text{si}} k \frac{k}{k_{\text{iK}}} + v_{\text{sn}} k_{\text{nT}} + v_{\text{sn}} k \frac{k}{k_{\text{nK}}} \right) \right. \\
& \quad + n^3 \left[v_{\text{sn}} k \frac{k}{k_{\text{nK}}} v_{\text{si}} k \frac{k}{k_{\text{iK}}} + v_{\text{sn}} k \frac{k}{k_{\text{nK}}} v_{\text{si}} k_{\text{iT}} + v_{\text{si}} k \frac{k}{k_{\text{iK}}} v_{\text{sn}} k_{\text{nT}} \right. \\
& \quad \left. + v_{\text{sn}} k_{\text{nT}} v_{\text{si}} k_{\text{iT}} + (v_{\text{sn}} k)^2 + (v_{\text{A}} k)^2 \chi \right] \\
& \quad + n^2 \left[\frac{1}{\gamma} (v_{\text{sn}} k)^2 (v_{\text{sn}} k_{\text{nT}} + v_{\text{sn}} k \frac{k}{k_{\text{nK}}}) - \frac{1}{\gamma} (v_{\text{sn}} k)^2 v_{\text{sn}} k_{\text{n}\rho} \right. \\
& \quad + (v_{\text{sn}} k)^2 (v_{\text{si}} k_{\text{iT}} + v_{\text{si}} k \frac{k}{k_{\text{iK}}}) - \frac{1}{\gamma} \chi (v_{\text{si}} k)^2 v_{\text{si}} k_{\text{i}\rho} \\
& \quad \left. + (v_{\text{A}} k)^2 \chi \left(v_{\text{si}} k_{\text{iT}} + v_{\text{si}} k \frac{k}{k_{\text{iK}}} + v_{\text{sn}} k_{\text{nT}} + v_{\text{sn}} k \frac{k}{k_{\text{nK}}} \right) \right] \\
& \quad + n \left[(v_{\text{A}}^2 k^2 \chi + \frac{1}{\gamma} v_{\text{sn}}^2 k^2) \right. \\
& \quad \cdot \left(v_{\text{sn}} k \frac{k}{k_{\text{nK}}} v_{\text{si}} k \frac{k}{k_{\text{iK}}} + v_{\text{sn}} k \frac{k}{k_{\text{nK}}} v_{\text{si}} k_{\text{iT}} + v_{\text{si}} k \frac{k}{k_{\text{iK}}} v_{\text{sn}} k_{\text{nT}} + v_{\text{sn}} k_{\text{nT}} v_{\text{si}} k_{\text{iT}} \right) \\
& \quad \left. - \frac{1}{\gamma} \chi (v_{\text{si}} k)^2 v_{\text{si}} k_{\text{i}\rho} (v_{\text{sn}} k_{\text{nT}} + v_{\text{sn}} k \frac{k}{k_{\text{nK}}}) - \frac{1}{\gamma} (v_{\text{sn}} k)^2 v_{\text{sn}} k_{\text{n}\rho} (v_{\text{si}} k_{\text{iT}} + v_{\text{si}} k \frac{k}{k_{\text{iK}}}) \right] \Big\}.
\end{aligned}$$

This is the dispersion relation (14).

B. Properties of the Dispersion Relation

The properties of thermal instability of one fluid approximation is briefly mentioned. According to Field (1965), the criterion of the condensation mode of the instability for the neutral component with or without the magnetic field is

$$\frac{\partial \Lambda_{\text{n}}}{\partial T_{\text{n}}} - \frac{\rho_{\text{n}0}}{T_{\text{n}0}} \frac{\partial \Lambda_{\text{n}}}{\partial \rho_{\text{n}}} < -k^2 \frac{K_{\text{n}0}}{\rho_{\text{n}0}}. \quad (\text{B1})$$

If the cooling becomes efficient with temperature diminishing, the system is thermally unstable. This is expressed at the first term on the left-hand side of equation (B1). If the cooling

becomes efficient according to the contraction, the system is also thermally unstable. This is expressed at the second term on the left-hand side. The thermal conduction smoothes the perturbation to suppress the instability. It is efficient at small-scale events. This is expressed at the term on the right-hand side.

Mathematically, whether the system is stable or not depends on whether the sign of the real part of the growth rate n is positive or negative. The system is unstable when the sign of the real part of n is positive. The sign of the real part of the solution of the dispersion relation is determined via algebra.

Similarly, the criterion of the condensation mode of the instability of the ion in the magnetic field is

$$\frac{\partial \Lambda_i}{\partial T_i} \left(1 + \gamma \frac{v_A^2}{v_{si}^2} \right) - \frac{\rho_{i0}}{T_{i0}} \frac{\partial \Lambda_i}{\partial \rho_i} < -k^2 \frac{K_{i0}}{\rho_{i0}} \left(1 + \gamma \frac{v_A^2}{v_{si}^2} \right). \quad (\text{B2})$$

If $\partial \Lambda_i / \partial T_i > 0$, the magnetic field always suppresses the instability. When $\partial \Lambda_i / \partial T_i < 0$, the criterion (B2) is rewritten as

$$-\frac{\rho_{i0}}{T_{i0}} \frac{\partial \Lambda_i}{\partial \rho_i} < - \left(\frac{\partial \Lambda_i}{\partial T_i} + k^2 \frac{K_{i0}}{\rho_{i0}} \right) \left(1 + \gamma \frac{v_A^2}{v_{si}^2} \right). \quad (\text{B3})$$

Then, the effect of the magnetic field on the instability depends on the sign of $\partial \Lambda_i / \partial T_i + k^2 K_{i0} / \rho_{i0}$. We note that this depends on the wave number k .

The critical wavelength, i.e., λ_F , above which the system is thermally unstable, is derived from equations (B1) for the neutral, or (B2) for the ion, respectively. The critical wavelength for the ion component depends on the magnetic field, while that for the neutral does not. The criterion (B1) is rewritten as

$$\frac{\lambda_F}{2\pi} = \frac{1}{k} = \sqrt{\frac{K_{n0}}{\rho_{n0}}} \cdot \left(\frac{\rho_{n0}}{T_{n0}} \frac{\partial \Lambda_n}{\partial \rho_n} - \frac{\partial \Lambda_n}{\partial T_n} \right)^{-\frac{1}{2}}, \quad (\text{B4})$$

the criterion (B2) is rewritten as

$$\frac{\lambda_F}{2\pi} = \frac{1}{k} = \sqrt{\frac{K_{i0}}{\rho_{i0}} \cdot \left(1 + \gamma \frac{v_A^2}{v_{si}^2} \right)} \times \left[\frac{\rho_{i0}}{T_{i0}} \frac{\partial \Lambda_i}{\partial \rho_i} - \frac{\partial \Lambda_i}{\partial T_i} \left(1 + \gamma \frac{v_A^2}{v_{si}^2} \right) \right]^{-\frac{1}{2}}, \quad (\text{B5})$$

respectively.

Moreover, the effect of the thermal conduction is mentioned. First, Observing to the conduction term $\nabla(K_n \nabla T_n)$ in equation (3) or the right-hand side of the criterion (B1), the conduction is more effective inversely proportionally to square of λ . Then, the conduction

becomes less effective at large scale. Second, according to the criterion (B1), the instability of the condensation mode prefers

$$\frac{\rho_{n0}}{T_{n0}} \frac{\partial \Lambda_n}{\partial \rho_n} \gg \frac{\partial \Lambda_n}{\partial T_n}.$$

The preference allows us to approximate

$$\begin{aligned} \lambda_F &\sim \sqrt{\frac{K_{n0}}{\rho_{n0}} \cdot T_{n0} \left[\rho_{n0} \frac{\partial \Lambda_n}{\partial \rho_n} \right]^{-1}} \\ &\sim \sqrt{\frac{K_{n0}}{\rho_{n0}} \cdot \frac{T_{n0}}{\Lambda_n}} \\ &= \lambda_{F(e)} \sqrt{\frac{K_{n0} T_{n0}}{(\lambda_{F(e)})^2} \cdot (\rho_{n0} \Lambda_n)^{-1}}. \end{aligned} \tag{B6}$$

According to equation (3), $K_{n0} T_{n0} / (\lambda_{F(e)})^2$ corresponds to the thermal conduction and $\rho_{n0} \Lambda_n$ to the cooling rate. This equation (B6) indicates that the critical wavelength $\lambda_{F(e)}$ is determined at the point where the effect of the thermal conduction is equivalent to that of the cooling. The larger the thermal conduction is, the more the system stabilizes especially at smaller scale, and then the critical wavelength is enlarged.

C. Normalization of the Dispersion Relation

We define the following quantities:

$$\begin{aligned} Y &\equiv \frac{n}{k_{n\rho} v_{sn}}, \quad X \equiv \frac{k}{k_{n\rho}}, \quad C_\nu \equiv \frac{\nu_{ni0}}{k_{n\rho} v_{sn}}, \\ \alpha_n &\equiv \frac{k_{nT}}{k_{n\rho}}, \quad \beta_n \equiv \frac{k_{n\rho}}{k_{nK}}, \quad \alpha_i \equiv \frac{k_{iT}}{k_{i\rho}}, \quad \beta_i \equiv \frac{k_{i\rho}}{k_{iK}}, \quad \kappa_{v_A} \equiv \frac{v_A}{v_{sn}}, \end{aligned}$$

and

$$\kappa_\rho \equiv \frac{k_{i\rho}}{k_{n\rho}}. \tag{C1}$$

According to $v_s^2 = \gamma(\mathcal{R}/\mu)T$,

$$\frac{v_{si}}{v_{sn}} = \sqrt{\frac{\mu_n T_{i0}}{\mu_i T_{n0}}}. \tag{C2}$$

Assuming $T_{i0} \sim T_{n0}$,

$$\frac{v_{si}}{v_{sn}} = \sqrt{\frac{\mu_n T_{i0}}{\mu_i T_{n0}}} \sim \sqrt{\frac{\mu_n}{\mu_i}} \equiv \mu_{ni}. \quad (C3)$$

Using these quantities, the dispersion relation (14) is normalized as follows:

$$\begin{aligned} & \left\{ Y^3 + Y^2(\alpha_n + X^2\beta_n) + YX^2 + \frac{X^2}{\gamma}(\alpha_n + X^2\beta_n - 1) \right\} \\ & \times \left\{ Y^3 + Y^2 \left(\mu_{ni}\kappa_\rho\alpha_i + \mu_{ni}\frac{\beta_i}{\kappa_\rho}X^2 \right) + Y(\mu_{ni}X)^2 + Y(\kappa_{vA}X)^2 \right. \\ & \quad \left. + \frac{1}{\gamma} \left(\mu_{ni}\kappa_\rho\alpha_i + \mu_{ni}\frac{\beta_i}{\kappa_\rho}X^2 \right) [(\mu_{ni}X)^2 + \gamma(\kappa_{vA}X)^2] - \frac{1}{\gamma}(\mu_{ni}X)^2\mu_{ni}\kappa_\rho \right\} \\ & = -\frac{C_\nu}{\chi} \left\{ Y^5 + Y^4 \left[\mu_{ni}\kappa_\rho\alpha_i + \mu_{ni}\frac{\beta_i}{\kappa_\rho}X^2 + \alpha_n + X^2\beta_n \right] \right. \\ & \quad + Y^3 \left[(\alpha_n + X^2\beta_n) \left(\mu_{ni}\frac{\beta_i}{\kappa_\rho}X^2 + \mu_{ni}\kappa_\rho\alpha_i \right) + X^2 + (\kappa_{vA}X)^2\chi \right] \\ & \quad + Y^2 \left[\frac{1}{\gamma}X^2(\alpha_n + X^2\beta_n - 1) + X^2 \left(\mu_{ni}\kappa_\rho\alpha_i + \mu_{ni}\frac{\beta_i}{\kappa_\rho}X^2 \right) - \frac{\chi}{\gamma}(\mu_{ni}X)^2\mu_{ni}\kappa_\rho \right. \\ & \quad \left. + (\kappa_{vA}X)^2\chi \left(\alpha_n + X^2\beta_n + \mu_{ni}\kappa_\rho\alpha_i + \mu_{ni}\frac{\beta_i}{\kappa_\rho}X^2 \right) \right] \\ & \quad + Y \left[\left(\kappa_{vA}^2X^2\chi + \frac{X^2}{\gamma} \right) (\alpha_n + X^2\beta_n) \left(\mu_{ni}\frac{\beta_i}{\kappa_\rho}X^2 + \mu_{ni}\kappa_\rho\alpha_i \right) \right. \\ & \quad \left. - \frac{1}{\gamma}\chi(\mu_{ni}X)^2\mu_{ni}\kappa_\rho(\alpha_n + X^2\beta_n) - \frac{1}{\gamma}X^2 \left(\mu_{ni}\kappa_\rho\alpha_i + \mu_{ni}\frac{\beta_i}{\kappa_\rho}X^2 \right) \right] \left. \right\} \quad (C4) \end{aligned}$$

We numerically solve this normalized dispersion relation (C4) in the main text.

REFERENCES

- Braun, R. & Kanekar, N. 2005, *A&A*, 436, 53
- Brogan, C. L., Zauderer, B. A., Lazio, T. J., Goss, W. M., De Pree, C. D., & Fasion, M. D. 2005, *AJ*, 130, 698
- Burkert, A., & Lin, D. N. C. 2000, *ApJ*, 537, 270
- Churchwell, E. B., et al. 2004, *ApJS*, 154, 322
- Davis, R. J., Diamond, P. J., & Goss, W. M. 1996, *MNRAS*, 283, 1105

- Dieter, N. H., Welch, W. J., & Romney, J. D. 1976, *ApJ*, 206, L113
- Diamond, P. J., Goss, W. M., Romney, J. D., Booth, R. S., Kalberla, P. M. W., & Mebold, U. 1989, *ApJ*, 347, 302
- Faison, M. D., Goss, W. M., Diamond, P. J., & Taylor, G. B. 1998, *AJ*, 116, 2916
- Faison, M. D., & Goss, W. M. 2001, *AJ*, 121, 2706
- Field, G. B. 1965, *ApJ*, 142, 531
- Frail, D. A., Weinberg, J. M., Cordes, J. M., & Mathers, C. 1994, *ApJ*, 436, 144
- Gibson, S. J., Taylor, A. R., Dewdney, P. E., & Higgs, L. A. 2000, *ApJ*, 540, 851
- Heiles, C. 1997, *ApJ*, 481, 193
- Inutsuka, S., & Sano, T. 2005, *ApJ*, 628, 155
- Kamaya, H., & Nishi, R. 2000, *ApJ*, 543, 257
- Koyama, H., & Inutsuka, S. 2002, *ApJ*, 564, 97
- Langer, W. D. et al. 1995, *ApJ*, 453, 293
- Mestel, L., & Spitzer, L., Jr. 1956, *MNRAS*, 116, 503
- Meyer, D. M., & Blades, J. C. 1996, *ApJ*, 464, L179
- Nakano, T. 1976, *PASJ*, 28, 355
- Nakano, T. 1979, *PASJ*, 31, 697
- O'Dell, C. R., McCullough, P. R., & Meixner, M. 2004, *AJ*, 128, 2339
- Rodríguez, L. F., Goss, W. M., & Williams, R. 2002, *ApJ*, 574, 179
- Ulmschneider, P. 1970, *A&A*, 4, 144
- Watson, C. et al. 2004, *ApJ*, 608, 274
- Wolfire, M. G., Hollenbach, D., McKee, C. F., Tielens, A. G. G. M. & Bakes, E. L. O. 1995, *ApJ*, 443, 152

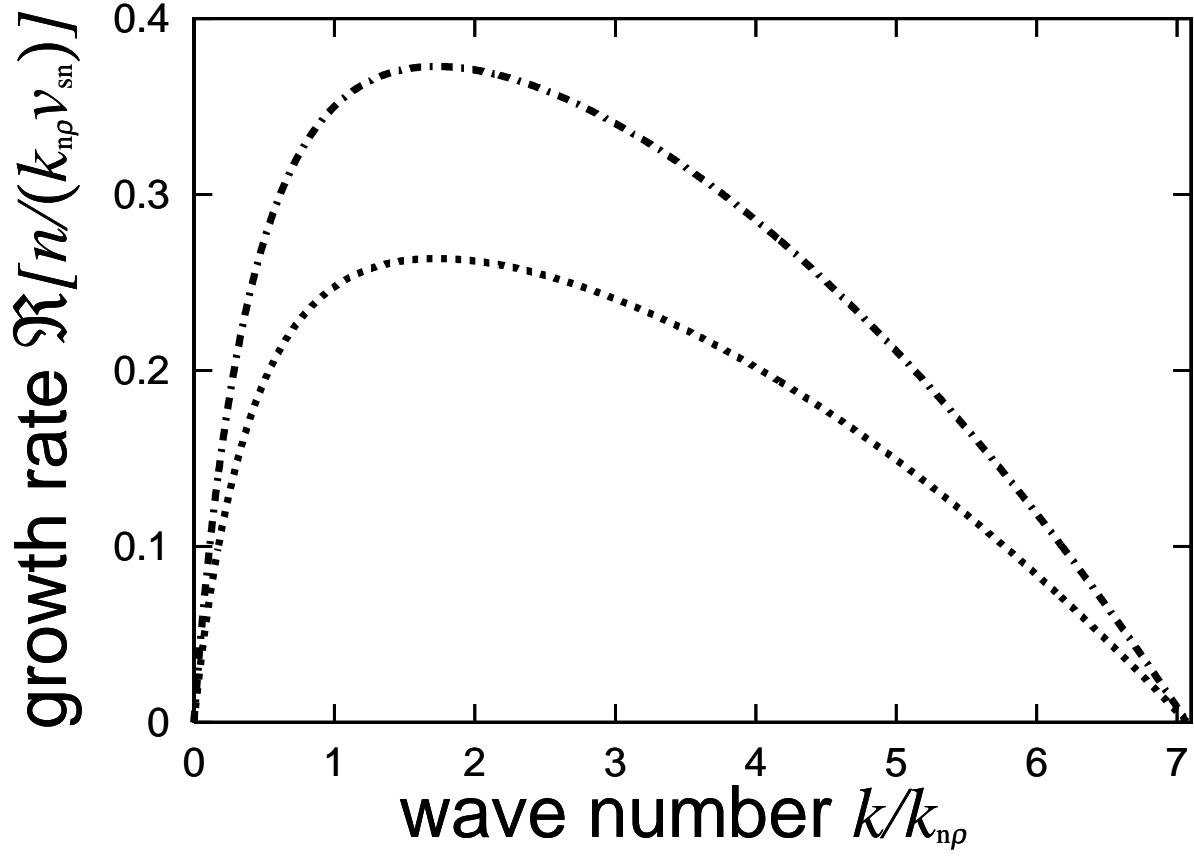


Fig. 1.— Growth rates of each condensation mode of the ion component (the dot-dashed curve) and the neutral component (the dashed one), when $B = 0$ and $\nu_{ni0} = 0$. The dot-dashed curve corresponds to fully ionized fluid and dashed one to totally neutral fluid. The horizontal axis is the normalized wave number k/k_{np} . The vertical axis corresponds to the normalized growth rate $\Re[n/(k_{np}v_{sn})]$.

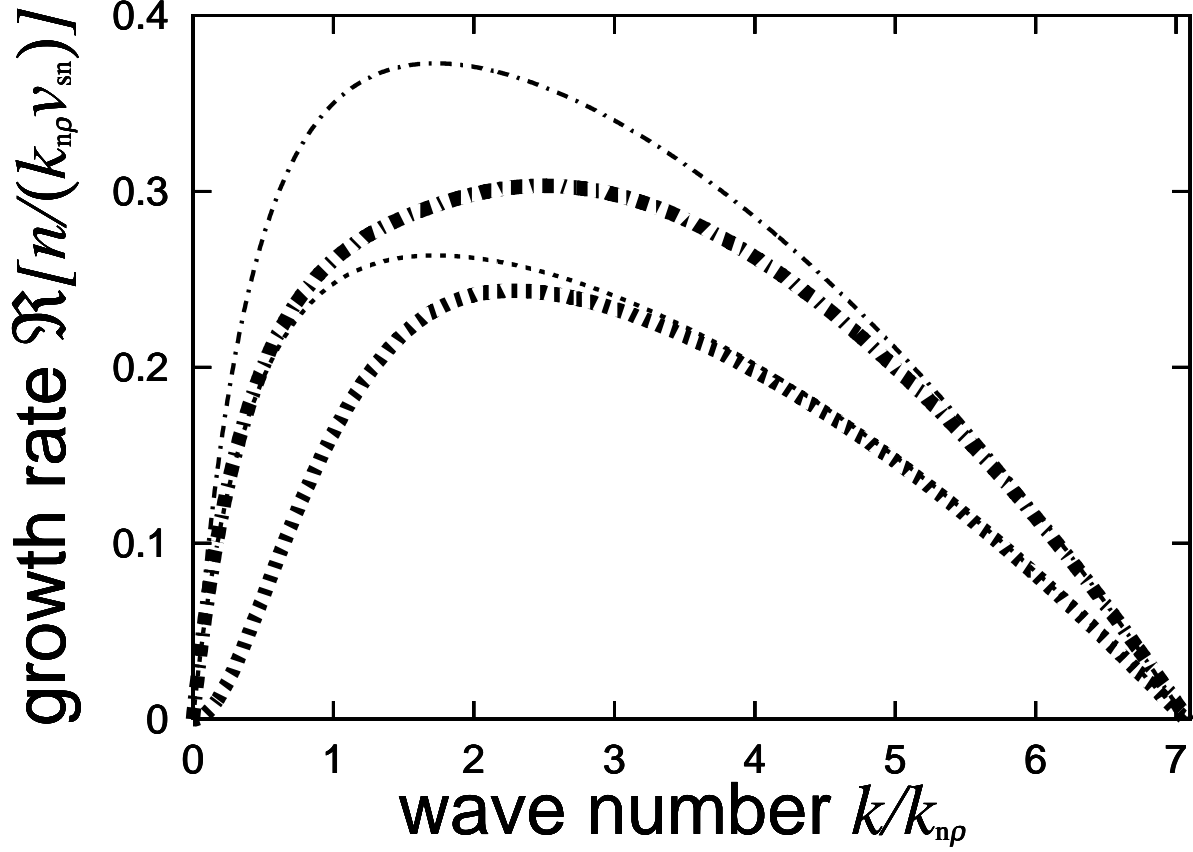


Fig. 2.— Growth rates of the condensation mode for the instability characterized by μ_n (the thick dashed curve) and μ_i (the thick dot-dashed curve), when $v_A/v_{sn} = 0$ and $\nu_{ni0}/(k_{np}v_{sn}) = 0.03$. The horizontal axis is the normalized wave number k/k_{np} . The vertical axis corresponds to the normalized growth rate $\Im[n/(k_{np}v_{sn})]$. This figure also corresponds to the case that the fluid moves along the magnetic field line. For comparison, there are also displayed condensation modes of the ion component (the thin dot-dashed curve) and the neutral component (the thin dashed curve) when $B = 0$ and $\nu_{ni0} = 0$, as well as Figure 1.

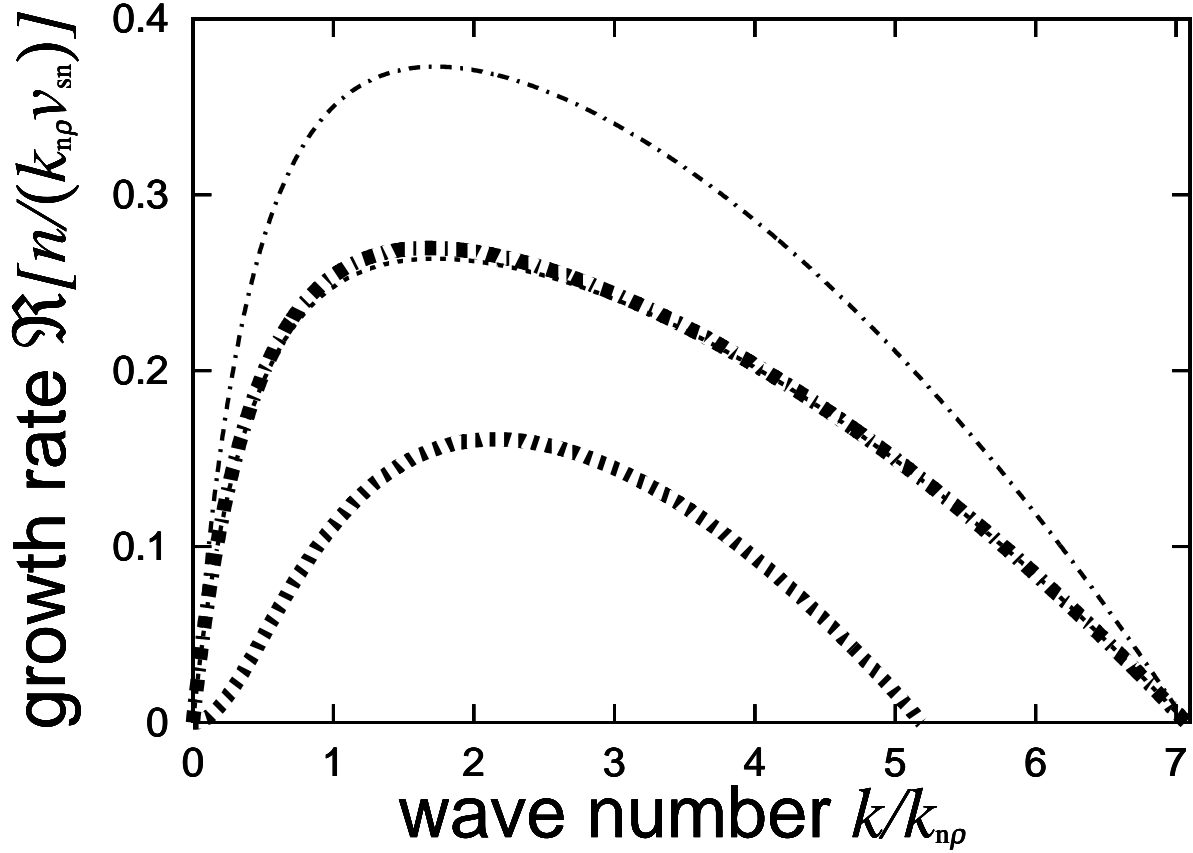


Fig. 3.— Growth rates of the condensation mode for the instability characterized by μ_n (the thick dot-dashed curve) and μ_i (the thick dashed curve), when $v_A/v_{\text{sn}} = 0.6$ and $\nu_{\text{ni}0}/(k_{n\rho}v_{\text{sn}}) = 0.03$. The horizontal axis is the normalized wave number $k/k_{n\rho}$. The vertical axis corresponds to the normalized growth rate $\mathfrak{R}[n/(k_{n\rho}v_{\text{sn}})]$. The difference between Figures 2 and 3 is the magnetic field strength. For comparison, there are also displayed condensation modes of the ion component (the thin dot-dashed curve) and the neutral component (the thin dashed curve) when $B = 0$ and $\nu_{\text{ni}0} = 0$, like Figure 2.

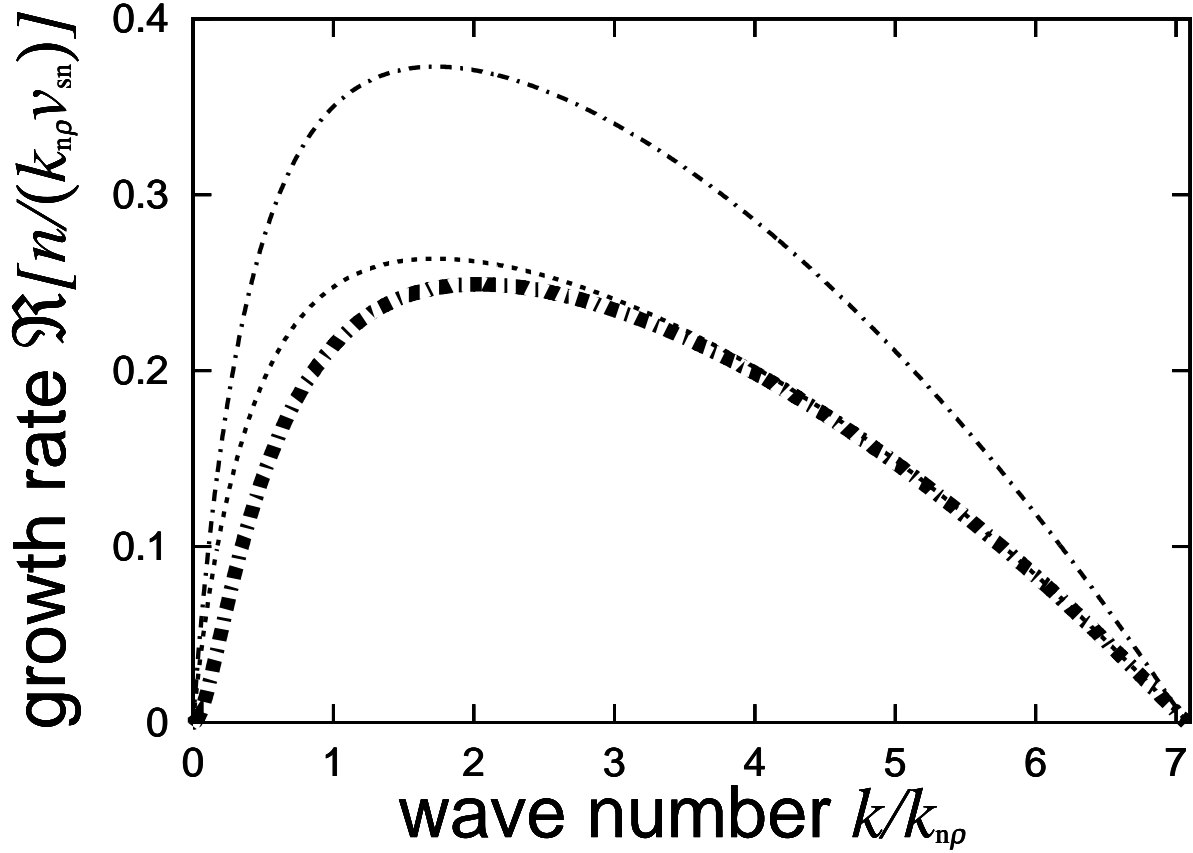


Fig. 4.— Growth rates of the condensation mode for the instability characterized by μ_n (the thick dot-dashed curve), when $v_A/v_{sn} = 600$ and $\nu_{ni0}/(k_{n\rho}v_{sn}) = 0.3$. The mode of μ_i is completely stabilized by the magnetic field and does not appear in this figure. The horizontal axis is the normalized wave number $k/k_{n\rho}$. The vertical axis corresponds to the normalized growth rate $\mathfrak{R}[n/(k_{n\rho}v_{sn})]$. For comparison, there are also displayed condensation modes of the ion component (the thin dot-dashed curve) and the neutral component (the thin dashed curve) when $B = 0$ and $\nu_{ni0} = 0$ like Figure 2.

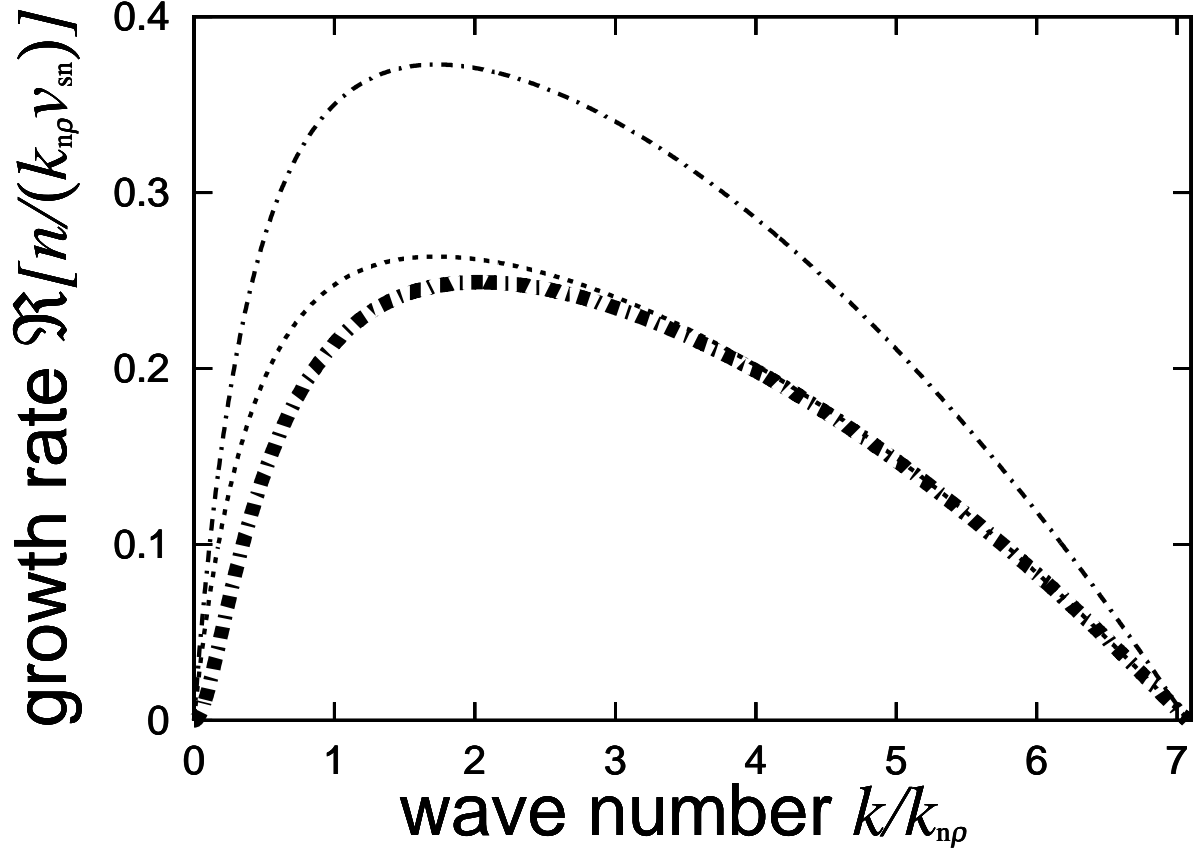


Fig. 5.— Growth rates of the condensation mode for the instability characterized by μ_n (the thick dot-dashed curve), when $v_A/v_{sn} = 6000$ and $\nu_{ni0}/(k_{n\rho}v_{sn}) = 0.3$. The mode of μ_i is completely stabilized by the magnetic field and does not appear in this figure. The horizontal axis is the normalized wave number $k/k_{n\rho}$. The vertical axis corresponds to the normalized growth rate $\Im[n/(k_{n\rho}v_{sn})]$. The difference between Figures 4 and 5 is the magnetic field strength. For comparison, there are also displayed condensation modes of the ion component (the thin dot-dashed curve) and the neutral component (the thin dashed curve) when $B = 0$ and $\nu_{ni0} = 0$ like Figure 2.

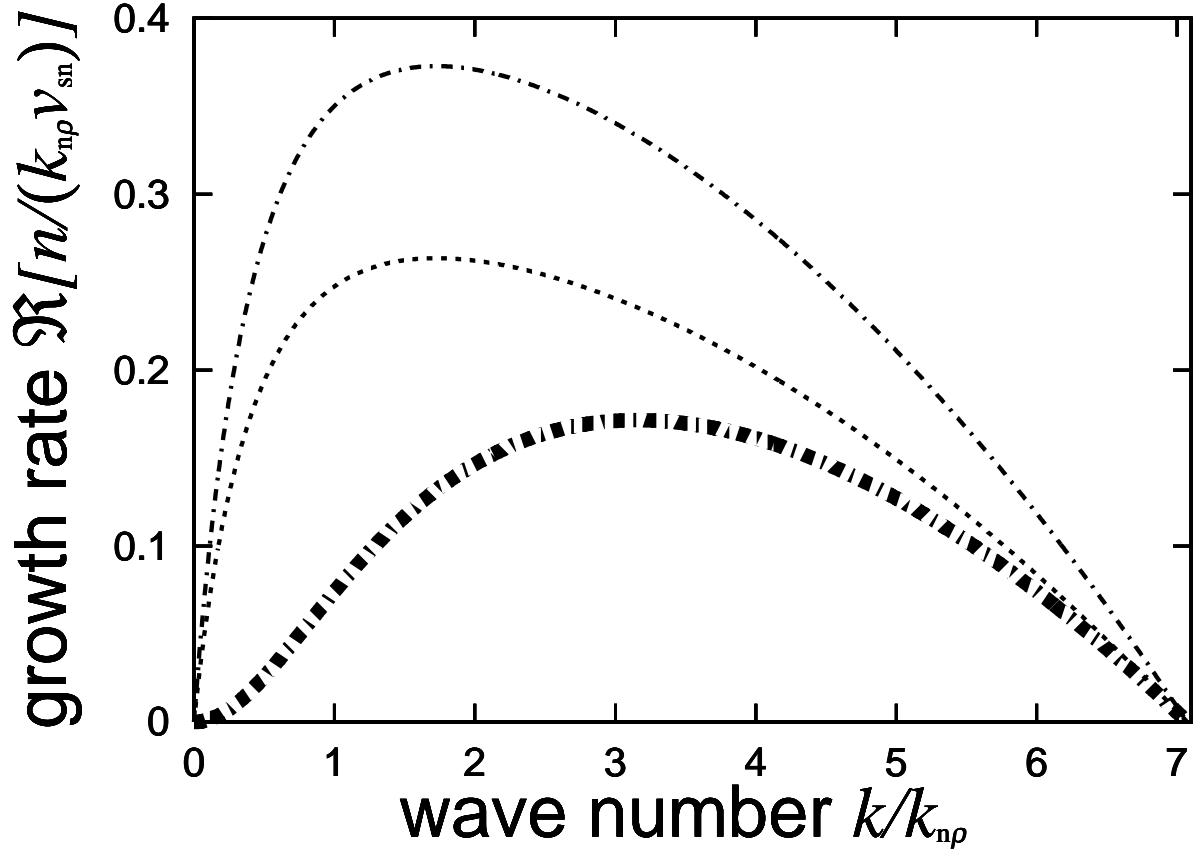


Fig. 6.— Growth rates of the condensation mode for the instability characterized by μ_n (the thick dot-dashed curve), when $v_A/v_{sn} = 600$ and $\nu_{ni0}/(k_{n\rho}v_{sn}) = 5$. The mode of μ_i is completely stabilized by the magnetic field and does not appear in this figure. The horizontal axis is the normalized wave number $k/k_{n\rho}$. The vertical axis corresponds to the normalized growth rate $\Im[n/(k_{n\rho}v_{sn})]$. The difference between Figure 4 and Figure 6 is the friction strength. For comparison, there are also displayed condensation modes of the ion component (the thin dot-dashed curve) and the neutral component (the thin dashed curve) when $B = 0$ and $\nu_{ni0} = 0$.

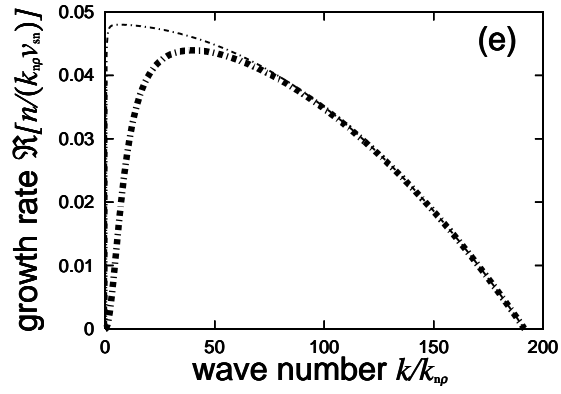
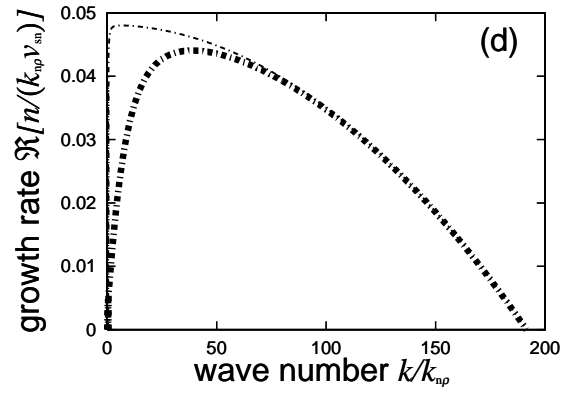
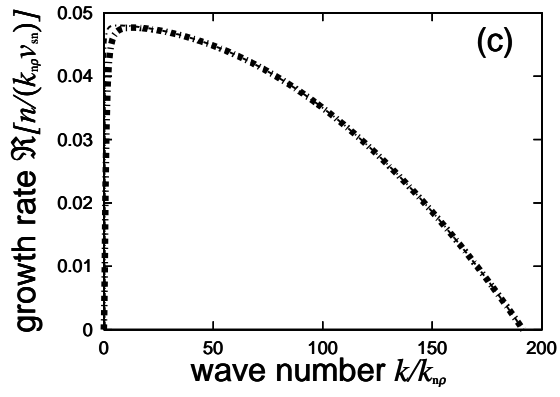
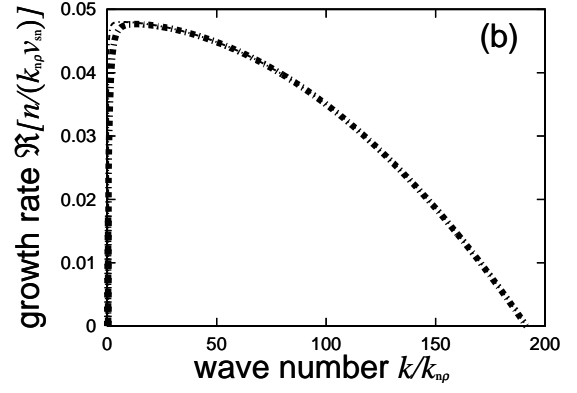
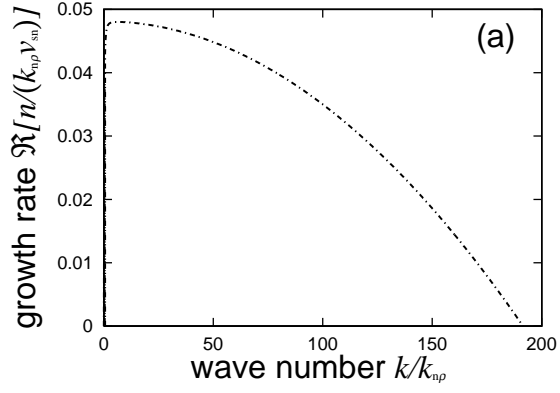


Fig. 7.— Growth rates of the condensation mode for the instability in the typical H I region, where $T = 100$ K and $n_{\text{neutral}} = 71.9 \text{ cm}^{-3}$. These panels show the case when $f_{\text{CII}} = 10^{-2}$ and $\chi = 10^{-6}$. The other parameters are assumed as $\langle \sigma v \rangle = 2 \times 10^{-9} \text{ cm}^3 \text{ s}^{-1}$, $K = 4.9 \times 10^3 \text{ erg cm}^{-1} \text{ s}^{-1} \text{ K}^{-1}$, $A_{\text{C}} = 3 \times 10^{-4}$, $\mu_n = 1$, $\mu_i = 1/2$, $\gamma = 5/3$. These panels are different in the strength of the magnetic field B and the friction. (a) both of B and the friction are zero; (b) both of B and the friction are the assuming typical values, i.e., $B = 10^{-6}$ Gauss (the thick dot-dashed curve); (c) B is hundred times as the assuming typical value, while the friction the assuming typical value (the thick dot-dashed curve); (d) B is the typical value, while the friction is hundred times as the assuming typical value (the thick dot-dashed curve); (e) both of B and the friction are hundred times as the assuming typical values (the thick dot-dashed curve). For comparison, there are also plotted the condensation mode when $B = 0$ and $\nu_{\text{ni}0} = 0$ (the thin dot-dashed curve) in each panel but (a). The horizontal axis is the normalized wave number $k/k_{\text{n}\rho}$. The vertical axis corresponds to the normalized growth rate $\Re[n/(k_{\text{n}\rho}v_{\text{sn}})]$. It is evaluated that $k_{\text{n}\rho} = 2.43 \text{ pc}^{-1}$ and $k_{\text{n}\rho}v_{\text{sn}} = 9.28 \times 10^{-14} \text{ s}$. It is noted that $\alpha_n = 0.920$, $\alpha_i = 920000$, $\beta_n = 2.19 \cdot 10^{-6}$, $\beta_i = 2.73 \cdot 10^{-7}$, $\kappa_{v_A} = 219$, $C_\nu = 0.775$, $\kappa_\rho = \chi/\mu_{\text{ni}}^2 = 5 \cdot 10^{-7}$, according to our notation summarized in Appendix C.

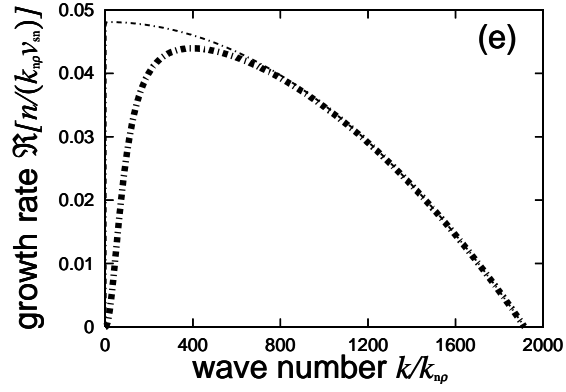
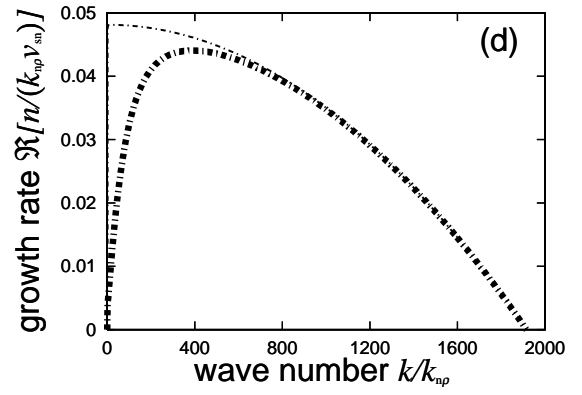
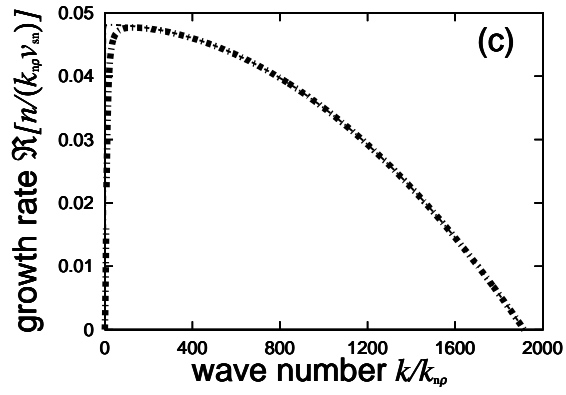
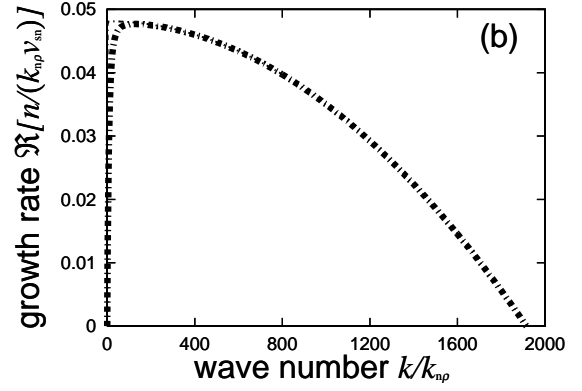
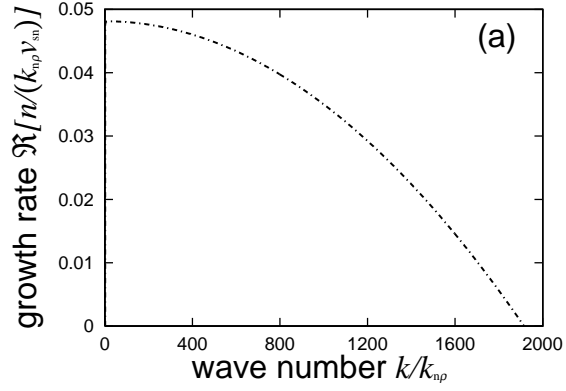


Fig. 8.— Growth rates of the condensation mode for the instability in the typical H I region, where $T = 100$ K and $n_{\text{neutral}} = 71.9 \text{ cm}^{-3}$. These panels show the case when $f_{\text{CII}} = 10^{-4}$ and $\chi = 10^{-6}$. The other parameters are assumed as $\langle \sigma v \rangle = 2 \times 10^{-9} \text{ cm}^3 \text{ s}^{-1}$, $K = 4.9 \times 10^3 \text{ erg cm}^{-1} \text{ s}^{-1} \text{ K}^{-1}$, $A_{\text{C}} = 3 \times 10^{-4}$, $\mu_n = 1$, $\mu_i = 1/2$, $\gamma = 5/3$. These panels are different in the strength of the magnetic field B and the friction. (a) both of B and the friction are zero; (b) both B and the friction is the assuming typical values, i.e., $B = 10^{-6}$ Gauss (the thick dot-dashed curve); (c) B is hundred times as the assuming typical value, while the friction the assuming typical value (the thick dot-dashed curve); (d) B is the typical value, while the friction is hundred times as the assuming typical value (the thick dot-dashed curve); (e) both of B and the friction are hundred times as the assuming typical values (the thick dot-dashed curve). For comparison, there are also plotted the condensation mode when $B = 0$ and $\nu_{\text{ni}0} = 0$ (the thin dot-dashed curve) in each panel but (a). The horizontal axis is the normalized wave number $k/k_{\text{n}\rho}$. The vertical axis corresponds to the normalized growth rate $\Re[n/(k_{\text{n}\rho}v_{\text{sn}})]$. It is evaluated that $k_{\text{n}\rho} = 0.0243 \text{ pc}^{-1}$ and $k_{\text{n}\rho}v_{\text{sn}} = 9.28 \times 10^{-16} \text{ s}$. Here, $\alpha_n = 0.920$, $\alpha_i = 920000$, $\beta_n = 2.19 \cdot 10^{-8}$, $\beta_i = 2.73 \cdot 10^{-9}$, $\kappa_{v_A} = 219$, $C_\nu = 77.5$, $\kappa_\rho = \chi/\mu_{\text{ni}}^2 = 5 \cdot 10^{-7}$.

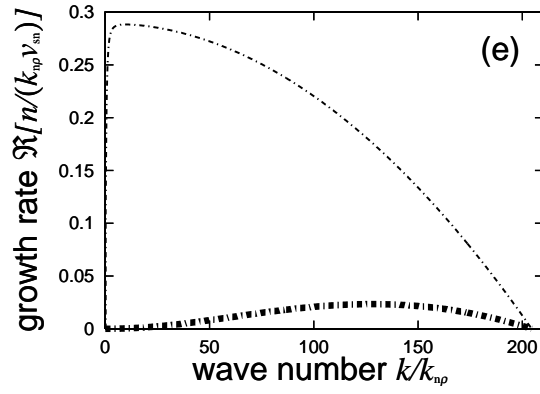
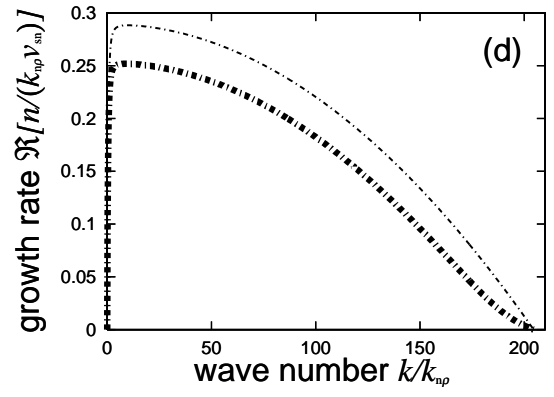
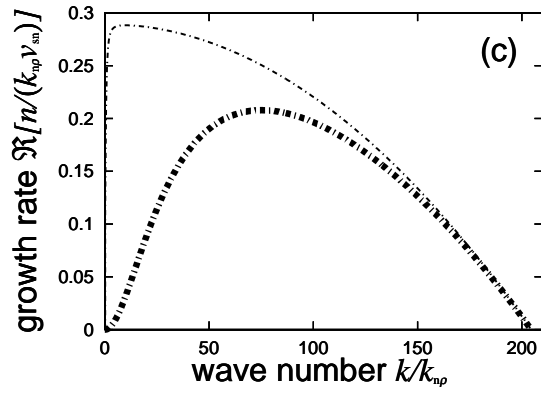
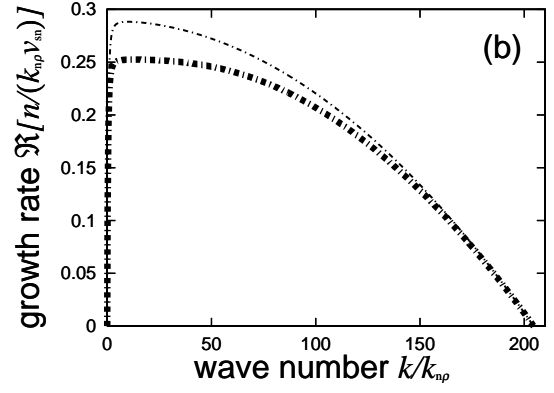
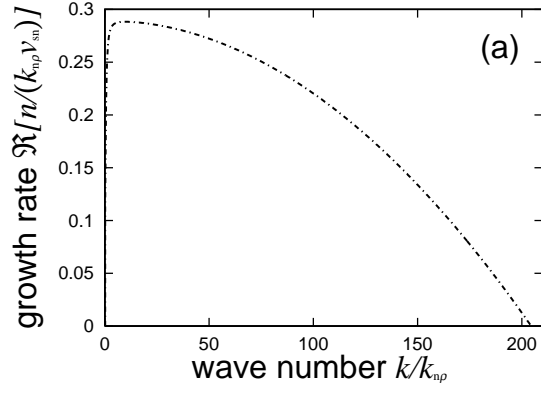


Fig. 9.— Growth rates of the condensation mode for the instability in the typical H I region, where $T = 100$ K and $n_{\text{neutral}} = 71.9 \text{ cm}^{-3}$. These panels show the case when $f_{\text{CII}} = 10^{-2}$ and $\chi = 10^{-2}$. The other parameters are assumed as $\langle \sigma v \rangle = 2 \times 10^{-9} \text{ cm}^3 \text{ s}^{-1}$, $K = 4.9 \times 10^3 \text{ erg cm}^{-1} \text{ s}^{-1} \text{ K}^{-1}$, $A_{\text{C}} = 3 \times 10^{-4}$, $\mu_n = 1$, $\mu_i = 1/2$, $\gamma = 5/3$. These panels are different in the strength of the magnetic field B and the friction. (a) both of B and the friction are zero; (b) both of B and the friction are the assuming typical values, i.e., $B = 10^{-6}$ Gauss (the thick dot-dashed curve); (c) B is hundred times as the assuming typical value, while the friction the assuming typical value (the thick dot-dashed curve); (d) B is the typical value, while the friction is hundred times as the assuming typical value (the thick dot-dashed curve); (e) both of B and the friction are hundred times as the assuming typical values (the thick dot-dashed curve). This case is the extreme one. For comparison, there are also plotted the condensation mode when $B = 0$ and $\nu_{\text{ni}0} = 0$ (the thin dot-dashed curve) in each panel but (a). The horizontal axis is the normalized wave number $k/k_{\text{n}\rho}$. The vertical axis corresponds to the normalized growth rate $\Re[n/(k_{\text{n}\rho}v_{\text{sn}})]$. It is evaluated that $k_{\text{n}\rho} = 12.8 \text{ pc}^{-1}$ and $k_{\text{n}\rho}v_{\text{sn}} = 4.90 \times 10^{-13} \text{ s}$. We adopt $\alpha_n = 0.517$, $\alpha_i = 51.7$, $\beta_n = 1.15 \cdot 10^{-5}$, $\beta_i = 1.44 \cdot 10^{-6}$, $\kappa_{v_A} = 2.19$, $C_\nu = 1470$, $\kappa_\rho = \chi/\mu_{\text{ni}}^2 = 5 \cdot 10^{-3}$.